Physical properties of the semiconductor-electrolyte interface

V. M. Arutyunyan

State University, Erevan

Usp. Fiz. Nauk **158**, 255–291 (June 1989)

This review discusses the structure of an electrical double layer formed at the semiconductor–electrolyte interface, as well as the energy states and imperfections in the electrolyte and on the semiconductor surface. A considerable part of the review is devoted to the results of investigations of photoelectric effects, luminescence, reflection, and electroreflection at this interface. The quantum size effects which occur in semiconductor electrodes and in colloids and the injection of hot electrons into an electrolyte are discussed in later sections of the review. A classification of photoelectrochemical cells is given and current data are provided on devices for conversion of solar or laser radiation energy into electrical and chemical energy.

1. INTRODUCTION

In the last 15 years a new subject of electrochemical physics[1)] has appeared and grown: it represents photoelectrochemistry of semiconductors developing on the basis of the concepts, ideas, and experimental methods adopted earlier not only in physical chemistry and chemical physics, but primarily in the physics of solids and semiconductors, surface physics, semiconductor microelectronics, and materials science.

At present photoelectrochemistry of semiconductors covers a wide range of border problems, is growing explosively, is stimulating discoveries and studies of new materials, and promises interesting applications in various sometimes unexpected branches of modern technology, including electronics, energetics, and control systems. Improvements in light sources should make it possible to use, for example, lasers in order to create the required topology of the surfaces of semiconductors immersed in electrolytes and to compete successfully with the available hologram recording methods. The energy crisis of the seventies has stimulated studies of photoelectrochemical solar cells of different types based on semiconductor photoelectrodes. One can quote also other examples of the application of successful ideas from photoelectrochemistry or semiconductors. These applications and the fundamentals of this new branch of science are discussed, for example, in monographs of Morrison[1] and of Gurevich and Pleskov[2], and in the review of Gerischer[3] in which the literature published to the end of 1980 is covered. Later work is discussed in more recent reviews.[4–7] A bibliography of work on this subject covering 1975–1983 can be found in Ref. 8. This book[8] fails, as is often the case, to give a full account of the work of Soviet authors; the gap is largely filled by the bibliographies in Refs. 2 and 4–6 and by the Proceedings of the All-Union Conferences on Photocatalytic Conversion of Solar Energy held in Novosibirsk in 1983 and in Leningrad in 1987, as well as of the Conference on Renewable Energy Sources held in 1985 in Erevan.[9–11]

2. STRUCTURE OF AN ELECTRICAL DOUBLE LAYER FORMED AT THE SEMICONDUCTOR–ELECTROLYTE INTERFACE

The semiconductor–electrolyte interface (SEI) is a more complex system than the interface between two different semiconductors. The different types of conduction (electronic and ionic) and the different aggregate states of the components in contact (solid, electrolyte) give rise to specific physical and physicochemical properties of this phase boundary, although one can easily establish a number of analogies with semiconductor heterojunctions and *p-n* junctions and with Schottky barriers at the semiconductor–metal interfaces.

A thermodynamic analysis of the processes at the SEI based on the generally known physical ideas and principles helps to understand and describe various ionic and electronic exchange processes in both phases and at the interface. As usual, the electrochemical potential (Fermi level) is the same in all parts of the system if it is in equilibrium. Nonequilibrium currents appear as a result of spatial variation of the Fermi level.

The electrochemical potentials of both phases are measured relative to the vacuum level. In this reference system the energies of affinity to an electron and a hole, and the values of the Fermi level in the semiconductor are negative relative to the vacuum level. It is known that the potential of the normal hydrogen electrode,[2)] which is in equilibrium at the interface because of the reaction

$$H^+ + e \rightleftharpoons \frac{1}{2} H_2, \tag{2.1}$$

lies 4.44 V below the vacuum level when the pressure of gaseous hydrogen above the electrolyte is 1 atm and the activity of the H^+ ions in the electrolyte is 1 mol/liter. Any potential in an electrochemical cell is usually found by comparison with a potential of the normal hydrogen electrode or other standard electrodes, which are therefore known as the reference electrodes. The latter include saturated calomel or silver/silver-chloride electrodes, the potentials of which relative to the normal hydrogen electrode are 0.24 and 0.22 V, respectively.

When a semiconductor is immersed in a liquid electrolyte, a thermodynamic equilibrium is as usual established by various electronic and ionic exchange processes at the interface. Electric charges of opposite sign (electrons, holes, ions) accumulate on both sides of the SEI creating an electric field. Charge accumulation at the interface creates an electrical double layer and a certain potential known as the Galvani potential which compensates for the difference between the chemical potentials of the two phases in contact.[3)] The electrode potential is then the sum of the Galvani potential, ohmic losses in the bulk of the semiconductor, and possible contact potentials inside the semiconductor.[4)] The internal resistance is reduced by the use of saturated solu-

0038-5670/89/060521-22$01.80
© 1989 American Institute of Physics

tions of electrolytes with ion concentrations of the order of 10^{21} cm^{-3} (1 M solutions).

At very low densities of the surface states at the SEI the structure of the double layer at the interface has the form shown in Fig. 1. The loss of electrons from the semiconductor to the electrolyte creates a positive space charge region in the surface layer of the semiconductor. On the other side of the SEI this positive charge is compensated by negative ions present in the electrolyte (Fig. 1b). A dense layer of ions adjoining directly the SEI is known as the Helmholtz layer and its thickness is governed by the size of the practically immobile ions "attracted" to the SEI (this thickness is of the order of several angstroms). On the electrolyte side the Helmholtz layer is followed by a space charge region known as the Gouy–Chapman layer. This layer forms in practice only in electrolytes with a low ion concentration and in the case of a 1 M solution its thickness is approximately 1 Å.

It therefore follows that an electrical double layer at the SEI consists of three components: the space charge region in the semiconductor, the Helmholtz layer, and the space charge region in the electrolyte. Consequently, the total potential drop across the SEI is the sum of the potential drops in these three regions (Fig. 2a).

The formation of the double layer is also influenced by dipoles that form near the SEI, due to the formation of polar bonds between the semiconductor surface and adatoms and due to oriented adsorption of the solvent molecules, as well as the dipole moment associated with a redistribution of the electron density on the semiconductor surface. The last dipole moment exists also on the surface of a solid even when it is in contact with vacuum. These dipoles do not affect the electrode charge, but they do contribute an additional potential jump which is very sensitive to the quality of the surface treatment and to the composition of the ambient medium. This additional potential jump is usually included in the potential across the Helmholtz layer φ_H.

We shall now turn our attention back to the interface along the direction of the axes of the potentials used in the physics of semiconductors and in electrochemistry. In electrochemistry it is usual to measure potentials from the potential of a reference electrode, which is identical (apart from a constant) with the potential deep inside the solution $U(-\infty)$. In the physics of semiconductors the potential is assumed to be zero in the bulk of the semiconductor (i.e., at $+\infty$). Therefore, in calculation of the Galvani potential the application of a certain electrical bias (polarization) to the electrode changes this potential by $\Delta\varphi_g$ (Fig. 2b)

$$\Delta\varphi_G = \Delta\varphi_e + \Delta\varphi_H - \Delta\varphi_s. \tag{2.2}$$

In the ideal case the value of $\Delta\varphi_H$ is close to zero (the subscripts s and e are used for the semiconductor and electrolyte).

In the case when $\varphi_s = 0$ the electrode potential φ measured relative to a reference electrode is known as the flat-band potential φ_{fb}. The potential on the semiconductor surface is then equal to the potential in the bulk of the semiconductor. If $\varphi_s > 0$, the energy bands of the semiconductor are bent downward, but if $\varphi_s < 0$ they are bent upward. In the case of an n-type semiconductor a surface layer with an accumulation of the majority carriers is formed if $\varphi_s > 0$, whereas in a p-type semiconductor it appears if $\varphi_s < 0$. Depletion and inversion layers are possible when these inequalities are reversed. We shall consider the specific case of an n-type semiconductor in which immersion in an electrolyte results in the formation of a depletion layer (Mott–Schottky layer) because of immobile ionized donor centers.

The density of the Fermi gas (specifically, the gas of electrons) is related to the electrochemical potential μ by[13]

$$n = \frac{2}{\hbar^3}\left(\frac{m_n^* kT}{2\pi}\right)^{3/2} F_{1/2}\left(\frac{\mu}{kT}\right), \tag{2.3}$$

where

$$F_{1/2}\left(\frac{\mu}{kT}\right) = \frac{2}{\sqrt{\pi}}\int_0^\infty \frac{\xi^{1/2}\,d\xi}{\exp[\xi-(\mu/kT)]+1}, \quad \xi = \frac{\mathscr{E}-\mathscr{E}_c}{kT},$$

m_n^* is the effective mass of an electron, k is the Boltzmann constant; T is the absolute temperature; e is the electron charge; $\mathscr{E}$ is the energy; $\mathscr{E}_c$ is the energy corresponding to the bottom of the conduction band. The Fermi integral $F_{1/2}$ cannot be calculated explicitly. In most cases this integral is described by the following asymptotes:

$$F_{1/2}\left(\frac{\mu}{kT}\right) = \exp\frac{\mu}{kT}, \qquad \frac{\mu}{kT} \leqslant 0, \tag{2.4a}$$

$$= \frac{4}{3\sqrt{\pi}}\left(\frac{\mu}{kT}\right)^{3/2}, \qquad \frac{\mu}{kT} > 1{,}3. \tag{2.4b}$$

We shall discuss below the solutions of the Boltzmann equations for these two asymptotes. Using Eq. (2.4b) for the case of a degenerate n-type semiconductor, we can find the distribution of the potential from the Boltzmann equation:

$$\frac{d^2\varphi}{dx^2} = -\frac{e}{\varepsilon_0\varepsilon_s}\left[N_D - N_A - \frac{4n_0}{3\sqrt{\pi}}\left(\frac{e\varphi}{kT}\right)^{3/2}\right]; \tag{2.5}$$

here, N_D is the donor concentration, N_A is the acceptor concentration, and n_0 is the thermal density of electrons. The donors and acceptors are assumed to be completely ionized. Selecting zero of the potential to be in the interior of the semiconductor, we can reduce Eq. (2.5) to a differential

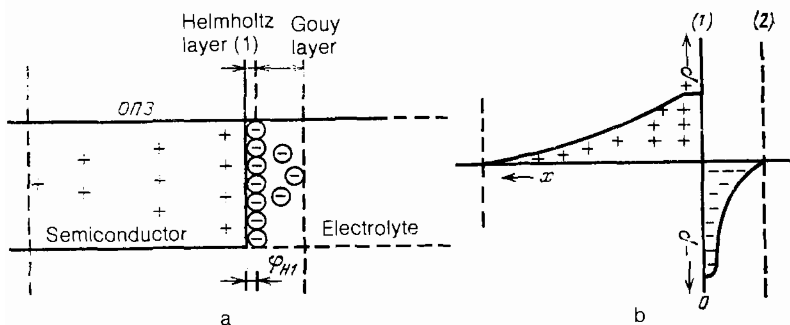

FIG. 1. Electrical double layer of a semiconductor–electrolyte interface.

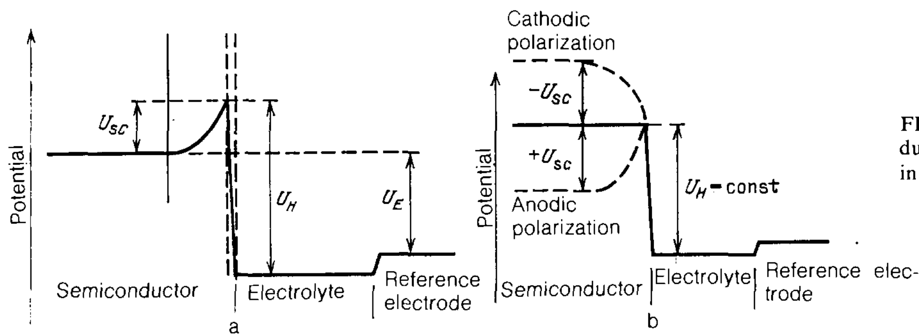

FIG. 2. Distribution of the potential at a semiconductor–electrolyte interface in equilibrium (a) and in the presence of polarization (b).[12]

equation for the Weierstrass function. If we limit the series for this function to its first term, we find that the expression for the potential becomes

$$\varphi=\frac{\varphi_s}{[1+(x/L^*)]^4}, \tag{2.6}$$

where

$$L^*=5{,}156\frac{L_D}{(Y^*)^{1/4}}, \tag{2.7}$$

$$L_D=\left(\frac{kT\varepsilon_0\varepsilon_s}{e^2n_0}\right)^{1/2},\quad Y^*=\frac{e\varphi_s}{kT}, \tag{2.8}$$

and L_D is the Debye screening length. It follows from Eq. (2.6) that the potential falls nonexponentially with depth in a degenerate semiconductor.

The distribution of the potential φ in the case described by Eq. (2.4a) is found by solving the self-consistent Poisson–Boltzmann equation

$$\frac{d^2\varphi}{dx^2}=-\frac{e}{\varepsilon_0\varepsilon_s}\left[p_0\exp\left(-\frac{e\varphi}{kT}\right)-n_0\exp\frac{e\varphi}{kT}+N_D-N_A\right], \tag{2.9}$$

where p_0 is the thermal density of holes.

The first integral in Eq. (2.9) can be calculated exactly: the expression for the electric field on the semiconductor surface E_s is written in the form

$$E_s=\pm\frac{kT}{eL_D^i}F(Y^*,\lambda^*), \tag{2.10}$$

where

$$L_D^i=\left(\frac{\varepsilon_0\varepsilon_n kT}{2e^2n_i}\right)^{1/2},\quad \lambda^*=\left(\frac{p_0}{n_0}\right)^{1/2}.$$

The function $F(Y^*,\lambda^*)$, defined by

$$F(Y^*,\lambda^*)=\{\lambda^*[\exp(-Y^*)-1]+(\lambda^*)^{-1}(\exp Y^*-1)+[\lambda^*-(\lambda^*)^{-1}]Y^*\}^{1/2}, \tag{2.10'}$$

is tabulated in Ref. 13; graphs of the function are given in Refs. 14 and 15. The total charge per unit surface area of the semiconductor Q_s is

$$Q_s=\mp\frac{kT\varepsilon_0\varepsilon_s}{eL_D^i}F(Y^*,\lambda^*), \tag{2.11}$$

so that the differential capacitance of the space charge region in the semiconductor, reduced to a unit area of the SEI, is

$$C_s=\frac{\varepsilon_0\varepsilon_s}{2L_D^iF(Y^*,\lambda^*)}|(\lambda^*)^{-1}(\exp Y^*-1)^{-1}-\lambda^*[\exp(-Y^*)-1]|. \tag{2.12}$$

In the case of a depletion layer $N_D\gg n_i$, N_A; $n_0\approx N_D$; $p_0\ll N_D$ in the region $0\leqslant x\leqslant W$, we have

$$\varphi(x)=-\frac{eN_D}{2\varepsilon_0\varepsilon_s}(x-W)^2. \tag{2.13}$$

The thickness of the space charge region is

$$W=\left(\frac{2\varepsilon_0\varepsilon_s|\varphi_s|}{eN_D}\right)^{1/2}=L_D(2Y^*)^{1/2} \tag{2.14}$$

and it is proportional to the Debye length L_D. The expression for the capacitance becomes

$$C_s^{-2}(\text{см}^4/\Phi^2)=\frac{2L_D}{\varepsilon_0^2\varepsilon_s^2}(|Y^*|-1)=\frac{1.41\cdot10^{32}}{\varepsilon_sN_D}\left(\varphi-\varphi_{fb}-\frac{kT}{e}\right). \tag{2.15}$$

This dependence is known as the Mott–Schottky law. According to Eq. (2.15), we have $S_s^{-2}\to0$ when $\varphi_s=0$, i.e., extrapolation of the experimentally determined curves (Fig. 3) can be used to find the flat-band potential φ_{fb} by measuring the capacitance. It follows from Fig. 3 that the values of φ_{fb} for n- and p-type semiconductors are different.

The distribution of the potential in the space charge region in the electrolyte is found from the self-consistent equation

$$\frac{d^2\varphi}{dx^2}=\frac{2ec_0}{\varepsilon_0\varepsilon_e}\,\text{sh}\,\frac{\varphi(x)-\varphi_e}{kT}, \tag{2.16}$$

which in contrast to Eq. (2.9) can be solved exactly. The electric field E_e at the boundary between the diffusion layer in the electrolyte and the Helmholtz (dense) layer is

$$E_e=\left(\frac{8c_0kT}{\varepsilon_0\varepsilon_e}\right)^{1/2}\text{sh}\,\frac{e\psi'}{2kT}. \tag{2.17}$$

The notation used in Eqs. (2.16) and (2.17) is as follows: c_0 is the bulk (volume) concentration of ions inside the solution, $\varepsilon_0\varepsilon_e$ is the permittivity of the electrolyte; φ_e is the potential inside the electrolyte; Ψ' is the potential on the outer plane surface of the Helmholtz layer measured relative to the potential well inside the electrolyte. In the case of an electrolyte containing multiply charged ions the expression for E_e becomes more complicated [see, for example, Eq. (3.36) in Ref. 2].

In the simplest case the differential capacitance of the SEI represents a series connection of the capacitances of the semiconductor C_s, of the Helmholtz layer C_H, and of the electrolyte C_e.

3. ENERGY STATES IN THE ELECTROLYTE AND THEIR PARTICIPATION IN TRANSPORT PROCESSES

The ions in the electrolyte can be in reduced or oxidized states. The transition from one state to the other involves an electron and is described by

$$[\text{Ox}]+se\rightleftharpoons[\text{Red}],$$
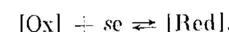

where s is the number of electrons participating in this reaction. Ions of the same metal in two different charge states

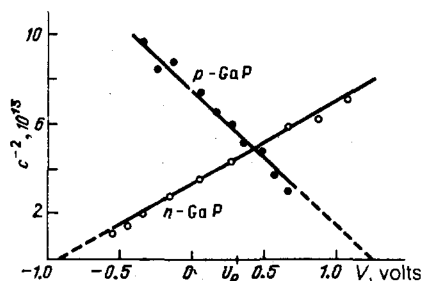

FIG. 3. Mott-Schottky dependences for GaP in a 0.1-N H_2SO_4 solution.[12]

(for example, Fe^{2+} and Fe^{3+}) may form a reduction–oxidation (redox) system in the electrolyte across which electrons may be transported from the electrolyte to the semiconductor and vice versa.

In contrast to crystalline solids, where the energy states (levels) have unique values (for example, the position of any impurity center, the bottom of the conduction band, or the top of the valence band), in liquid media the interaction of electrons and ions with their environment means that we can speak only of the average values of their characteristic energies, since both ions and molecules interact with the ambient medium which is a polar liquid. Fluctuations of these interactions shift the energy levels in either direction from the most probable value.

The positions of the energy levels of a redox pair in the electrolyte are governed by the ionization energy of the reduced states and by the electron affinity of the oxidized states. Time-average fluctuations of the energy states give for each component of a redox pair a Gaussian distribution of the energy of the level near its average characteristic value if fluctuations of a solvation shell are harmonic. The distribution is characterized by what is known as the reorientation (or reorganization) energy λ_R. It is assumed that a rapid transition of an electron does not affect the solvation shell. According to the Franck–Condon principle the characteristic times of the electron transitions are of the order of 10^{-15} s. The system formed by an ion and the surrounding liquid electrolyte "particle" contains "heavier" components than an electron. This system cannot follow the motion of the electron and the exchange of energy between them does not take place in the short electron transition time. It follows from the Franck–Condon principle that this transition is not accompanied by any changes in the energy ($\mathscr{E} = \mathscr{E}'$) and this applies also to the emission or absorption of photons (i.e., the transition is nonradiative), the interaction with vibrational modes, plasmons, etc. The solvation shell is modified subsequently. This requires the energy λ_R which is proportional to the quantity $a^{-1}(\varepsilon_{\rm opt}^{-1} - \varepsilon_{\rm st}^{-1})$, where a is the radius of an ion, and $\varepsilon_{\rm opt}$ and $\varepsilon_{\rm st}$ are the optical-frequency and static permittivities of the electrolyte.

The value of λ_R represents a fraction of an electron volt or even a few electron volts, so that in some cases the energy levels of a redox pair may "penetrate" not only the range of energies corresponding to the band gap of the semiconductor, but even above the bottom of the conduction band of the semiconductor or below the top of its valence band (Fig. 4). The Gaussian distribution of the energy levels in the electrolyte has a half-width $2(\lambda_R kT)^{1/2}$. The values of λ_R are different in the bulk of the electrolyte and at the interface. In the latter case the transport of charge across the interface results in changes in the half-space occupied by the electrolyte, whereas in the case of the solution the changes apply throughout the ambient space. This is the reason for the different values of λ_R in the case of heterogeneous and homogeneous reactions.

The Fermi level (electrochemical potential) of a redox pair F_R obeys the Nernst equation

$$F_{\rm R} = F_{\rm R}^0 + kT \ln \frac{c_{\rm ox}}{c_{\rm red}}, \tag{3.1}$$

where $c_{\rm ox}$ and $c_{\rm red}$ are the concentrations of the oxidized and reduced components of the pair in the electrolyte. If $c_{\rm ox} = c_{\rm red}$, the Fermi level $F_R = F_R^0$ lies half-way between the most probable energy levels of the oxidized and reduced states of an ion. Figures 4b and 4c show schematically the positions of the Fermi level of a redox pair F_R in the case when $c_{\rm ox} \neq c_{\rm red}$.

Some of the above assumptions may, in principle, be disobeyed. A more general microscopic approach is needed to develop a theory of electron states and transitions in electrolytes. A very interesting alternative approach is proposed by Khan and Bockris.[16]

Variation of pH of an electrolyte shifts the energy positions of bands of the semiconductor and of redox pairs at a rate of 59 meV/pH (Nernst shift), which is due to an increase in the adsorption of hydroxyl groups on increase in pH. Figure 2 in Ref. 5 shows the positions of the energy bands of a semiconductor immersed in an aqueous electrolyte. This figure demonstrates a great variety of positions of the semiconductor band edges and of the energy of redox pairs relative to one another, which suggests that kinetic processes occur on each specific SEI. All these energy processes represent heterogeneous chemical reactions which are accompanied by the transfer of an electric charge across the

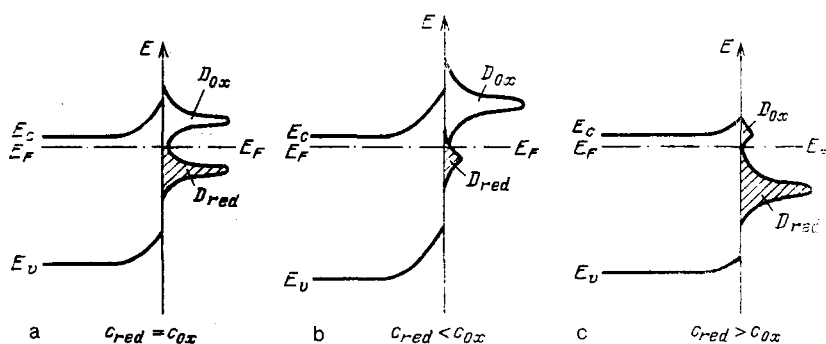

FIG. 4. Energy states in equilibrium expected for different concentrations.[12]

SEI. The energy processes and in particular the rate of charge transport from the semiconductor to the electrolyte and vice versa depend strongly on the difference between the electric potentials between the two phases. Therefore, in contrast to conventional chemical kinetics, where the important kinetic variables are the concentration and temperature, a major role is played by an independent variable representing the electrode potential.

A typical current-voltage characteristic of the SEI is shown in Fig. 5 for the case of *n*- and *p*-type GaAs in a 1-M solution of H_2SO_4. The continuous curves in this figure represent the characteristic in darkness and the dashed curves represent the same characteristic during illumination of the SEI. A phenomenological description of the electrode reactions, calculations of the electron transport current across the SEI, and the current-voltage characteristic of this interface have attracted many authors (see, for example, Refs. 2, 4, and 5). Studies have been made not only of the cases when there are direct electron transitions between the levels in the conduction or valence band and fluctuating electron levels in the electrolyte, but also the processes occurring in other ways, such as quantum-mechanical tunneling of carriers across the thin space charge region of the semiconductor, transport via surface states on the SEI, etc. The exceptionally great variety of possible situations means that we cannot assume that all the fundamental problems of electrochemical kinetics have already been solved. Further serious complications arise when it is necessary to allow for the participation of both allowed bands of the semiconductor in the electron reaction, as well as in calculations dealing with the processes accompanied by photoexcitation of the semiconductor and reagents in the electrolyte and by double injection of carriers from sensitizers into the semiconductor or by emission of hot electrons from the semiconductor into the electrolyte. Special attention should be given to the kinetics of the reactions which alter the composition of the surface layer of the semiconductor or cause its dissolution or corrosion (including photocorrosion). The resistance of various semiconductors to corrosion and photocorrosion has been investigated on many occasions. However, this is outside the scope of the present review (for further information see Refs. 1–5 and 17).

Figure 5 shows the current-voltage characteristics for low currents across the SEI. In the presence of strong anodic bias voltages the potential across the Helmholtz layer increases and there is also a considerable voltage drop across the space-charge region, which increases strongly the probability of impact ionization in this region.[18,19] This results in a rapid rise of the photocurrent followed by a saturation region. Hysteresis loops are then exhibited by the current-voltage characteristics in darkness and during illumination. The ratio of the values of the photocurrent in the region of rapid rise to the value before impact ionization gives approximately the multiplication coefficient. In fact, the ionization does occur when voltages $V \sim 2$–3 volts are applied to ZnO and TiO_2 surface layers. An even faster rise of the current in the range $V \gg 7$ volts is clearly due to the Zener breakdown. Eventually the number of ionization events reaches saturation and the resistance of the space charge region falls steeply.[18,19]

4. INFLUENCE OF IMPERFECTIONS ON THE SURFACE REACTIONS

Since the periodic potential of a crystal terminates at the SEI, the presence of dangling electron bonds, structure defects, etc. on the surface gives rise to states[20,21] which are best called interface electron states. They have an important influence on the processes occurring at the SEI.

Electrons and holes are captured by these surface states forming a surface electric charge which induces an opposite charge in the bulk of the semiconductor. Moreover, the surface states have a considerable influence on the kinetics of electron processes occurring at the SEI because they may act as additional recombination centers, trapping levels, and intermediate centers in the process of charge transport across the interface. Therefore, the existence of such states at the SEI frequently affects strongly the flow of the current across the interface and the various nonequilibrium processes (including the photoprocesses discussed below). The density of such states can reach 10^{14}–10^{13} cm^{-2} on the semiconductor surface. These states can be "fast" or "slow" from the point of view of relaxation of the charge and the processes governing the characteristic relaxation times vary greatly, beginning from the interaction with phonons and electrons in the solid and ending with diffusion across oxide films on the semiconductor. Therefore, there are usually several relaxation times. Statistics of the surface recombination processes has been developed thoroughly. Oxidation of an electrode during its dissolution in an electrolyte is called corrosion. Corrosion of semiconductors is usually enhanced by illumination of an electrode because this generates a large number of the minority carriers. The reactions on the semiconductor surface can vary greatly and they have been given much attention in the literature (see, for example, Refs. 1–5). We shall not consider the oxidation and dissolution of an electrode, especially as the description of the corrosion process at the SEI can be provided simply by an analogy with surface recombination processes and we can demonstrate the role of the surface states in prevention of photocorrosion of semiconductors.[1-5,17] A major role is played also by the surface states in heterogeneous catalysis and details on this topic can be found in Ref. 21.

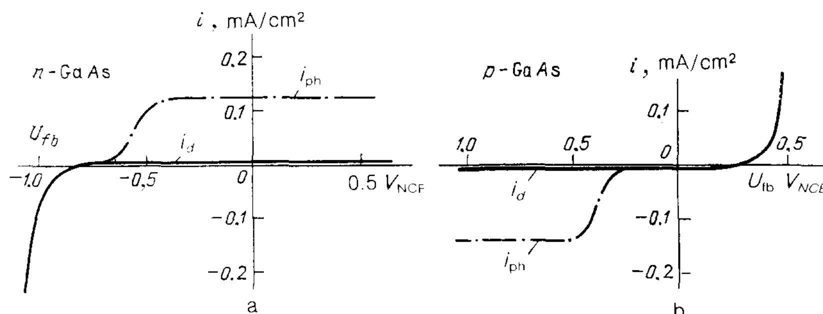

FIG. 5. Current-voltage characteristics of GaAs electrodes in a 1-N H_2SO_4 solution. The continuous curve represents the characteristic in darkness and the chain curve is the characteristic during illumination.[12]

The most widely used method for the determination of the density of the surface states at the SEI is measurement of differential capacitance C_{ss} (Refs. 2 and 22). Using an equivalent circuit describing the SEI, we can calculate the density of the surface states N_{ss}. Under certain conditions the value of C_{ss} can be greater than the semiconductor capacitance C_s or it may be comparable with the capacitance of the Helmholtz layer. A high density of the surface states N_{ss} may result in a redistribution of the potential in various layers associated with the SEI.

5. PHOTOELECTRIC EFFECTS AT THE SEMICONDUCTOR–ELECTROLYTE INTERFACE

We shall now briefly consider the effects which occur as a result of illumination of the SEI when the absorption of light in the electrolyte is weak. Illumination with photons of energies exceeding the width of the band gap of the semiconductor (i.e., corresponding to the fundamental absorption region of the semiconductor) results in generation of electron–hole pairs in the semiconductor. The depth of the absorption of light in the semiconductor, which is of the order of $1/\alpha$, where $\alpha(\omega)$ is the absorption coefficient, usually varies with the wavelength of light λ. Photogeneration of carriers in the surface layers of the semiconductor can alter radically the rates and nature of the physical and chemical processes occurring at the SEI.

Electron–hole pairs become separated in the space charge region: holes in an n-type semiconductor are transported by the electric field to the electrode surface and electrons are displaced deeper into the semiconductor. Gärtner[23] assumed that the dark current is zero and obtained the following expression for the absolute value of the photocurrent J_{ph}:

$$J_{ph}=eI_0\left[1-\frac{\exp(-\alpha W)}{1+\alpha L_p}\right]. \tag{5.1}$$

The rate of generation of electron–hole pairs $g(x)$ is $I_0\,\alpha\exp(-\alpha x)$. In Eq. (5.1) the symbol L_p is the diffusion length of holes and I_0 is the photon flux. If $(\alpha)^{-1}\gg W, L_p$, it follows from Eq. (5.1) that the photocurrent is proportional to $\alpha(W+L_p)$, but if $(\alpha)^{-1}\ll W$, it is equal to the maximum possible value of eI_0, i.e., all the photoholes contribute to the photocurrent. A more rigorous analysis was carried out in several other papers by a variety of methods (see, for example, Ref. 2).

The electrode potential φ changes as a result of illumination from the dark value φ_d to φ_i, which after a number of simplifying assumptions was found to be given by

$$\varphi_i=-\frac{kT}{e}\ln(1+\xi I_0), \tag{5.2}$$

where

$$\xi=\frac{\alpha L_p}{1+\alpha L_p}\left(\frac{D_n N_D}{\Lambda^0}+\frac{D_p p_0}{L_p}\right)^{-1}, \tag{5.3}$$

$$\Lambda^0=\sqrt{2}\,L_D\int_0^{|Y_0^*|^{1/2}}\exp(z^2)\,dz;$$

Y_0^* is the value of Y^* in the presence of an equilibrium potential (the subscripts n and p refer to electrons and holes).

It follows from Eq. (5.2) that in this simplified situation in the absence of surface recombination the photopotential in the space charge region is negative. This means that illumination of an n-type semiconductor reduces the potential drop in the space charge region and the energy bands are bent. In the case of a p-type semiconductor the bands are again bent as a result of illumination but the photopotential is positive. A linear rise of the absolute value of the photopotential on increase in the illumination intensity occurs, as predicted by Eq. (5.2), if $\xi\ll I_0^{-1}$. A further increase in the photon flux (illumination intensity) makes this dependence weak (logarithmic).

If αL_p and αW are much less than 1, a series expansion of the exponential function in Eq. (5.1) gives

$$\varphi-\varphi_{fb}=\frac{N_D}{2\varepsilon_0\varepsilon_s e}\left(\frac{J_{ph}}{\alpha I_0}\right)^2. \tag{5.4}$$

Extrapolation of the dependence J_{ph}^2 on φ and of the Mott–Schottky dependence to the point of intersection with the potential axis makes it possible to find the flat-band potential. This method is used widely in an analysis of the experimental data obtained for various materials. The values of the flat-band potential φ_{fb} for some oxide semiconductors can be found in, for example, Refs. 4 and 5. Equation (5.1) also readily yields the following expression for the quantum efficiency:

$$\eta=A_n(\hbar\omega-E_g)^{n/2}\left[L_p+\left(\frac{2\varepsilon_0\varepsilon_s|\varphi_s|}{eN_D}\right)^{1/2}\right], \tag{5.5}$$

which can be used to establish the nature of interband phototransitions in a semiconductor near the edge of the fundamental absorption band: in the case of direct transitions we have $n=1$, whereas for indirect transitions we find that $n=4$ (Refs. 24 and 25) and the value of A_n depends on such transitions.

The photoelectric effects at the SEI illuminated with photons of energies less than the width of the band gap of the semiconductor are of considerable interest. Such illumination corresponds to the impurity and exciton absorption regions. We shall cite the results of investigations carried out at the Erevan State University on TiO_2 and ZnO (Refs. 26–32) to demonstrate some characteristic features of the photocurrent spectra for the SEI and the photoconductivities of such systems. Reference to earlier work done at the Erevan State University, the results of which will be used below, can be found in Refs. 4 and 5. Some of the results have been presented at conferences.[9–11]

Figure 6 shows the photocurrent spectra of TiO_2 obtained in the impurity part of the spectrum. The long-wavelength photosensitivity can hardly be attributed to the conventional mechanism of the tunneling of bound holes from acceptor levels to the surface, because $\alpha<10^4$ and pairs are generated quite far from the surface. Acceptor impurity levels create a certain density of the surface states. Absorption of a photon of energy $h\nu<E_g$ transfers electrons from the surface states to the conduction band, where in the presence of a strong electric field generated in the space charge region these electrons tunnel into the bulk of the semiconductor. Similar results were obtained by us using the method of photoacoustic spectroscopy.[29] The widest impurity photosensitivity range was observed in the case of TiO_2:V. Atoms of vanadium were at levels located 2.1 eV below E_c. Investigations of the cathodoluminescence spectra of these samples[30] demonstrate that large complexes of vanadium and intrinsic defects of the TiO_2 lattice, particularly V_0^{-2}, are formed. Figure 6b shows the spectral dependences of the photocur-

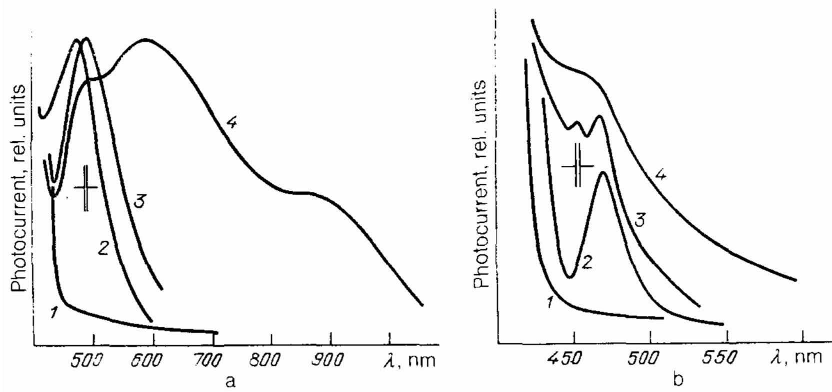

FIG. 6. Photocurrent spectra of polycrystalline TiO_2 doped with: a) Al (curve 1), Cr (curve 2), Mn (curve 3), and V (curve 4); b) Cr in concentrations of 0 at.% (curve 1), 0.1 at.% (curve 2), 1.0 at.% (curve 3), and 2.5 at.% (curve 4).

rent in undoped rutile and in TiO_2:Cr samples with different chromium concentrations (0.1–2.5 at.%) and these dependences demonstrate that in the impurity absorption region the photocurrent rises linearly on increase in the chromium concentration. Extrapolation of the long-wavelength edge of the photocurrent spectrum yields the values of the activation energy of acceptor levels. This dependence on the impurity concentration and also the width of the photocurrent band suggest that optical transitions do not occur from one level or even from several levels. We are most likely dealing with an impurity subband formed on the surface.

A comparison of the spectral dependences of the photoconductivity and photocurrent across the TiO_2–electrolyte interface shows that the former spectrum is shifted toward shorter wavelengths relative to the latter. This is a consequence of the formation of a region with a high electric field ($\sim 10^5$ V/cm) in the surface layer adjoining the SEI. This field may weaken greatly the role of surface recombination and enhance the proportion of the carriers which are generated in the interior of the semiconductor and participate in the various processes. Introduction of different impurities can be used to control the short-wavelength part of the spectrum.

The spectral dependences of the photoconductivity were obtained by us in the temperature range 77–300 K (Fig. 7). A steep fall of the photosensitivity was observed and the position of the minimum shifted toward lower wavelengths relative to the bulk exciton line: by 50 meV in the case of sample 1 and by 73 meV for sample 2. An increase in temperature (curves 2–4) broadened the main minimum and shifted it from 375.9 to 383 nm by analogy with the temperature-induced changes in the bulk exciton line exhibited by ZnO. The role of the surface was investigated by measurements of the photoconductivity of a ZnO single crystal. A brief chemical etching of a sample in a selective etchant not only shifted the maximum considerably toward longer wavelengths, but also altered the spectrum.

The minima and the high sensitivity to the surface treatment exhibited by these spectra (curves 2–4 in Fig. 7) on the long-wavelength side of the bulk exciton line demonstrated that the observed excitons were of surface origin. The photoconductivity spectra of moderately doped samples revealed

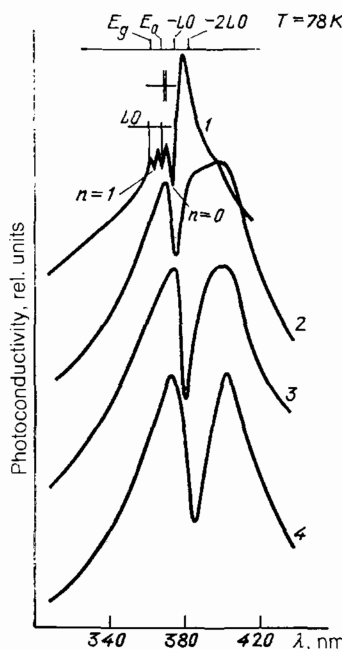

FIG. 7. Photoconductivity spectra of polycrystalline ZnO with $N_D - N_A \approx 10^{17}$ cm^{-3} (1) and 10^{18} cm^{-3} (2–4). $T = 78$ K (1, 2), 170 K (3), and 300 K (4).

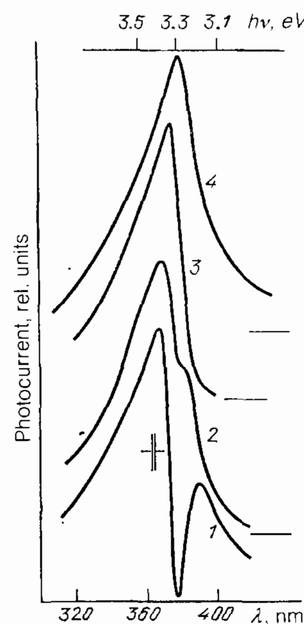

FIG. 8. Photocurrent spectra of the interface between a ZnO single crystal and an electrolyte subjected to various external voltages (V): 1) -0.5; 2) 0.45; 3) 0; 4) 2.5. $T = 300$ K.

the presence of both bulk and surface excitons. For example, a maximum at $\lambda = 367.8$ nm (curve 1 in Fig. 7) represented a bulk exciton line (its spectral position was the same for different single-crystal samples) and a minimum at 364 nm varied in synchronism with the main minimum. The separation between them was 90 meV, which was considerably higher than the LO phonon energy in a ZnO crystal (71 meV), whereas the first phonon replica of the bulk exciton was manifested by a steep fall on the short-wavelength side of the photoconductivity spectrum. The hypothesis of the surface nature of the observed exciton lines was supported by the observation that the positions of the lines attributed to the surface excitons varied from sample to sample, and as a function of the surface treatment. Changes in the spectral profiles were observed also when a light beam scanned the length of a sample in the presence of an inhomogeneous field. Measurements carried out by the scanning capacitance probe method showed that at high values of x (far from the region of rapid variation of the surface fields) there were two maxima at wavelengths ~ 380 and 393 nm. Illumination of the region where the surface potential was highest quenched the latter line. In this case the surface excitons were formed from carriers located in the appropriate surface bands. A similar investigation of the photoconductivity spectra at 80 K revealed bulk and quasi-two-dimensional (I with a carrier in a surface subband and II in a bulk subband) excitons and the band of quasi-two-dimensional excitons was quenched at low values of x.

The exciton nature of the photoconductivity bands at 370–375 nm was supported also by measurements of the photoconductivity using different polarizations of the incident light relative to the optic axis of ZnO. In view of the low value of the spin–orbit splitting it was found that at high temperatures two exciton lines were observed for $\mathbf{E}\perp\mathbf{c}$ and $\mathbf{E}\parallel\mathbf{c}$. The spectral maxima were shifted by ~ 0.04 eV, in agreement with the value of the splitting due to the influence of the hexagonal crystal field in ZnO. The maxima observed at 300 K were most likely due to dissociation of bulk excitons. The distribution of the maxima obtained for a specific polarization of light agreed with the energies of the A and C bulk excitons revealed by the reflection spectra.

Figure 8 shows the spectral dependences of the photocurrent obtained for an interface between ZnO and 0.1 N KCl and different anodic and cathodic polarizations. A minimum (dip) observed under a bias voltage of -0.5 V occurred at an energy of 3.28 eV which was ~ 90 meV less than E_g of ZnO at 300 K (3.37 eV). An increase in the bias voltage destroyed this minimum. Further increase in the band bending resulted in an overlap of this band with the bulk exciton absorption region, giving rise to a fairly wide band with its maximum (curve 4) shifted toward longer wavelengths compared with the interband transition region. When polarized light was used, the photocurrent maximum shifted by ~ 0.04 eV. All this evidence supported the exciton nature of the minimum (which could not be explained by impurity absorption in bulk or surface centers). It should also be mentioned that the position of the minimum was shifted toward energies lower than the bulk exciton line, which we attributed to the formation of surface excitons with a greater binding energy than bulk excitons. The energy position of the former varied from 3.28 to 3.2 eV depending on the state of the surface and on the degree of doping of the samples. An estimate of the critical field $E_{cr} = \mathscr{E}_{ex}/er_{ex}$ gave 3×10^5 and 5×10^5 V/cm for bulk and surface excitons, respectively. The exciton absorption coefficient was $\alpha_{ex} \sim 2 \sim 10^5$ cm^{-1} (300 K). Similar dependences were observed also in the spectral dependences reported for ZnO (Ref. 30) and CdTe (Refs. 10, 11, and 33).

6. LUMINESCENCE AT THE SEMICONDUCTOR–ELECTROLYTE INTERFACE

Recent years have seen a major increase of the interest in the luminescence investigation methods because previous studies of a whole range of materials have been hindered by difficulties encountered in fabrication of high-quality *p-n* junctions needed to apply sufficiently high electric fields and ensure high injection rates (these difficulties were due to self-compensation in such materials observed, for example, in II-VI semiconductors). A region with a high electric field in the vicinity of the SEI establishes favorable conditions for the observation of electroluminescence, photoluminescence, and cathodoluminescence, so there is no need to form a *p-n* junction. Studies of the SEI and of the surface layers of semiconductors by these methods have made it possible to understand the characteristics of surface recombination and of recombination in the space charge region, to study changes in the crystal structure as well as in the energy spectra of photons and plasmons in the surface part of the semiconductor, to detect excitons and donor–acceptor pairs, to observe various defects, and to investigate the role of redox pairs and various radicals in the generation of luminescence at the SEI. These investigations have become much easier because of the ease of variation of the surface potential in a very wide range. One can also quench or shift the wavelengths of various luminescence bands. Important information can be obtained from the time and temperature dependences of the luminescence and by investigation of the polarization effects.

It should be noted that in addition to the mechanisms of the electroluminescence generated as a result of injection of minority carriers from the electrolyte into the semiconductor, usually observed in the case of cathodic polarization, and of the electroluminescence resulting from the high-field effects in the anodic polarization case, we can also observe electroluminescence on reduction of an organic substance on a semiconductor photoelectrode.[42] Electrons from the conduction band are transferred to an excited state R^* of an organic substance and this is followed by a transition to the ground state R accompanied by emission of a photon. We shall concentrate our attention on the injection type of luminescence.

Studies of the luminescence at the SEI have already been made for systems based on the following semiconductors: II-VI compounds (ZnS, CdS, CdSe, ZnSe, ZnO, CdS_xSe_{1-x}), III-V compounds (GaP, GaAs), TiO_2, and $SrTiO_3$ (see Refs. 2–5, 18, 19, 30, 31, and 43–47 as well as the literature cited in them). A fairly efficient electrochemical "light-emitting diode" with an efficiency of 0.2–0.35% was described in Ref. 42 and it was reported that the electroluminescence maximum was observed at 460 nm when an aluminum-doped *n*-type zinc sulfide single crystal was placed in an electrolyte containing redox systems of the H_2O_2 and $S_2O_8^{2-}$ type, the total reduction of which resulted in injection of holes into the valence band of ZnS. Electrolu-

minescence under cathodic polarization conditions was observed[44] only in the case of injection of holes into the valence band of polycrystalline ZnO when $S_2O_8^{2-}$ was reduced. The injected holes recombined in these electrodes with electrons which accumulated near the surface. The injection of holes from simpler one-electron redox pairs $Fe^{2+/3+}$, $Ce^{3+/4+}$, and $Fe(CN)_6^{3-/4-}$ into the valence band of gallium arsenide was confirmed in Ref. 37 and in this case the electroluminescence was observed from 0.8 to 1.25 μm. It was established in Ref. 42 that double injection occurred in a fairly wide range of voltages[48] and the current was proportional to the square of ΔV, representing the difference between the applied voltage and the flat-band potential φ_{fb}. The electroluminescence intensity increased proportionally to the square of the current. These observations were made at voltages more negative than φ_{fb}. When the voltages were more positive than φ_{fb}, the current i rose exponentially with the applied voltage V. Significant electroluminescence was observed only when V was close to or more negative than φ_{fb}. The injection of holes into the valence band of ZnS and ZnO together with these features of the electroluminescence and of the current-voltage characteristic of the SEI were attributed in Refs. 34, 42, and 44 solely to the dissipation of the active radicals $SO_4\cdot$ or $\cdot OH$, formed as a result of chemical reduction of $S_2O_8^{2-}$ or H_2O_2. The half-width of the luminescence spectrum of ZnS:Al increased proportionally to the square root of the absolute temperature.[34]

The time dependences of the electroluminescence emitted by the ZnS:Al–electrolyte system were characterized by a fast (3.7 ns) exponential decay of the electroluminescence intensity I_L with time, followed by a slow component $I_L \propto t^{-1}$ ($\sim 1\,\mu$s). The slope of the slow component decreased on increase in the intensity of the exciting light. The time dependences of the electroluminescence intensity and current in the case of polycrystalline ZnO samples were also investigated.[44] The electroluminescence emitted by ZnO and TiO_2 was observed when these compounds were immersed in aqueous solutions of NaOH, KCl, H_2SO_4, NaCl + $Na_2S_2O_8$, etc. The electrode potential corresponding to the electroluminescence threshold was accompanied by the onset of a rapid rise of the current in the case of the dark current-voltage characteristics.[18,44] Changes in the electroluminescence brightness B at the interface of ZnO or TiO_2 with 1 M NaOH under an external bias voltage[47,44] obeyed a familiar dependence (see, for example, Refs. 24, 25, and 48)

$$B \propto \exp\left(-\frac{b}{V^{1/2}}\right), \qquad (6.1)$$

where b is a constant.

The spectral dependences of the electroluminescence intensity obtained for the ZnO electrodes investigated by us were reported in Refs. 18, 19, and 30. The spectra of a ZnO single crystal included three bands with maxima at ~380, 505, and 770 nm. The spectral dependences of the electroluminescence of polycrystalline ZnO (Fig. 9) indicated that doping with yttrium gave rise to a band with a maximum at $\lambda_{max} \approx 400$ nm, whereas doping with indium resulted in the appearance of two bands at $\lambda_{max} \sim 550$ and 670 nm. A band with a maximum at 530 nm was reported in Ref. 44 for ZnO:Co. Vacuum annealing of polycrystalline samples at high temperatures up to 1500°C also produced a band at $\lambda_{max} \approx 400$ nm. A wide peak at 550 nm was typical of ZnO

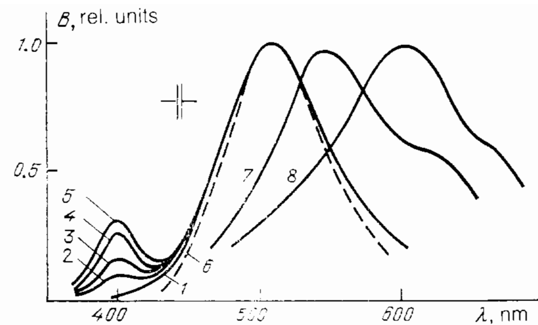

FIG. 9. Electroluminescence spectra of an interface between polycrystalline ZnO and a 1-N NaOH solution under a voltage $V = 10$ volts. Curve 1 represents undoped ZnO, whereas curves 2–4 represent samples doped with 0.25, 0.5, and 0.1 at.% of Y, respectively; 5) reduced at 1500 °C; 7), 8) doped with 0.5 and 1.0 at.% of In, respectively; 6) curve calculated using the Poisson distribution for the intensities of transitions assisted by LO phonons.

and was usually attributed to the luminescence emitted by donor–acceptor pairs (see, for example, Ref. 44).

The electroluminescence spectra obtained for TiO_2 had bands at $\lambda_{max} = 450$ and 530 nm after partial chemical reduction, whereas doping with Re and Nb gave rise to a band at $\lambda_{max} = 400$ nm.

Under the Zener breakdown conditions as a result of the anodic polarization, which was quite likely in our samples with the net impurity concentration $N_D - N_A \approx 10^{20}$ cm^{-3}, the process of radiative recombination could not be due to the tunneling of an electron and a hole because of their spatial separation. Holes accumulating at the surface cannot in practice recombine directly with electrons which are in reduced states in an electrolyte, since in our case the latter are located well above the top of the valence band. However, if there are surface states, these states may capture electrons from reduced fluctuating-energy levels in the electrolyte. Some of the electrons may tunnel to the conduction band and participate in the flow of the current, whereas the others may recombine radiatively with holes. Therefore, in our case the observed electroluminescence is generated at the surface. Only this explanation can account for the band at $\lambda_{max} = 505$ nm, common to all the ZnO samples (doped and reduced, single crystals and polycrystalline) due to intrinsic surface defects of ZnO. This is true also of the photoluminescence results, which we shall discuss later. The energy of such a surface LO phonon in ZnO is close to 65 meV, which differs little from the energy of a bulk LO phonon (71 meV). The depth of these levels is $\approx E_c - 0.6$ eV.

The level responsible for the peak at 400 nm lies ~0.1 eV below the bottom of the conduction band. On the other hand, in the case of ZnO:In the new band at longer wavelengths is clearly associated with the formation of $In_{Zn}V_{Zn}$ complexes characterized by an energy $E_v + 2.8$ eV. A band at $\lambda_{max} \approx 700$ nm is due to a level of iron at $E_c - 1.6$ eV. A strong band found at 380 nm for ZnO is assumed to be due to the formation of surface excitons.

A complex formed by a zinc vacancy V_{Zn} with Al is invoked in Ref. 36 to account for a luminescence maximum at $\lambda \approx 630$ nm (orange band) at the SEI formed by n-type ZnSe:Al.

Figure 10 shows the photoluminescence spectra of ZnO

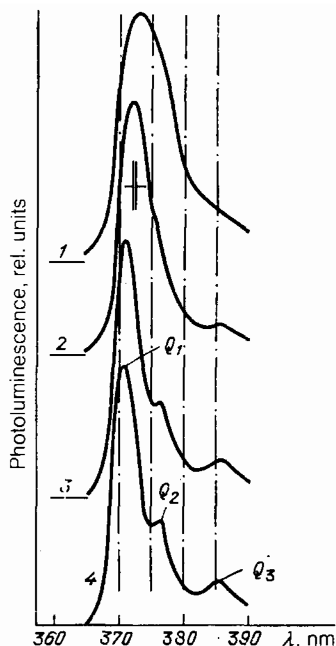

FIG. 10. Photoluminescence spectra of ZnO crystals subjected to excitation at different rates: 1) L_{max}; 2) 0.24; 3) L_{max}; 4)0.003 L_{max}. $T \approx 78$ K.

crystals (78 K) obtained at different excitation rates beginning from L_{max} (curve 1) right down to $0.003L_{max}$, where $L_{max} \approx 10^7$ W/cm^2 (Refs. 30, 45, and 46). Clearly, the line width was so large (the half-width was ~ 14 kT) that it could be regarded as an envelope of multiphonon transitions (at 78 K it should be possible to resolve readily the lines of the separate phonon replicas). In addition to the familiar band labeled Q_1, it was possible to resolve luminescence lines Q_2 and Q_3 with intensities dependent strongly on the state of the surface. The Q_1 band is usually attributed to the formation of an electron–hole liquid and radiative decay of biexcitons or due to the interaction of bound excitons with electrons. The electron–phonon interaction constant α^* for ZnO is 0.96 so that the exciton lifetime is short ($\tau \sim 10^{-9}$ s). Figure 11 shows the dependences of the intensity of a photoluminescence band (1) and of the photoresponse amplitude (2) on the rate of optical excitation L. It was found that

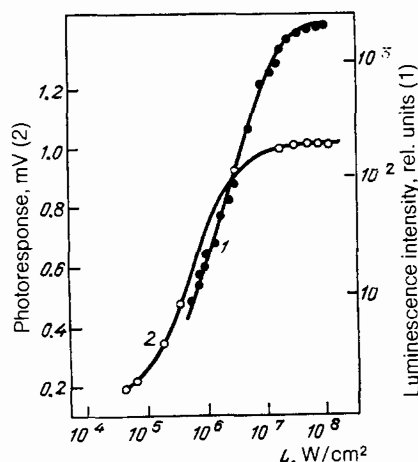

FIG. 11. Dependence of the intensity of the Q_3 photoluminescence band (1) and of the photoresponse amplitude (2) on the excitation rate L.

$I \propto L^n$, where $n = 1.6$. The reason for saturation of the absorption could be complete emptying of the valence band states near its top at some threshold excitation intensity. One could also postulate the formation of an energy gap near a resonance value of the quasimomentum. The excitation rates should in principle be sufficient for this purpose. We shall therefore assume that the Q_1 band (~ 371 nm) is due to inelastic scattering of excitons, particularly to the phonon branch of the polarization band, whereas the Q_2 and Q_3 bands (at ~ 376.5 and 385 nm) are due to quasi-two-dimensional and bound two-dimensional surface excitons.

Investigations of the influence of the surface on the intensities of the Q_2 and Q_3 luminescence bands demonstrated that an increase of the anodic bias potential quenched Q_3 and shifted Q_2 toward longer wavelengths. The application of small cathodic bias voltages (causing a reduction in the surface potential) resulted in enhancement of the Q_2 band. An increase of the external cathodic bias from 0.5 to 5 V quenched both bands. Similar changes in their intensities were observed when the concentration and the nature of the donor centers were altered. It should be noted that Q_2 was less affected by the surface potential than Q_3 (Ref. 30).

An investigation of the angular distribution of the intensities of the Q_2 and Q_3 bands demonstrated (Fig. 12) an almost spherical distribution of the radiation of the Q_2 band which predominated when the electrode was subjected to an anodic bias. Under cathodic bias voltages the Q_3 band dominated the luminescence spectrum and the emitted radiation was highly directional. When temperature was increased to 300 K the Q_1 line was quenched completely (Fig. 13). The Q_3 band could thus be attributed to radiative decay of excitons localized directly at the surface of the investigated crystal in a layer of thickness less than the Bohr exciton radius. The Q_2 excitons, formed from an electron in the conduction band and a hole in a two-dimensional surface subband, did not create luminescence with the same strong directionality.

The influence of polarization of the luminescence emitted by cadmium selenide electrodes (wurtzite structure) was reported in Ref. 35. The photoluminescence spectrum consisted of two bands at energies close to E_g, but differing from one another by ~ 0.022 eV. The band at the lower energy appeared for **E**⊥**c**, whereas the one at the higher energy was independent of the polarization of the exciting radiation. These luminescence bands were attributed to the splitting of the Γ_9 and Γ_7 valence subbands of CdSe.

Quenching of the photoluminescence in the space-

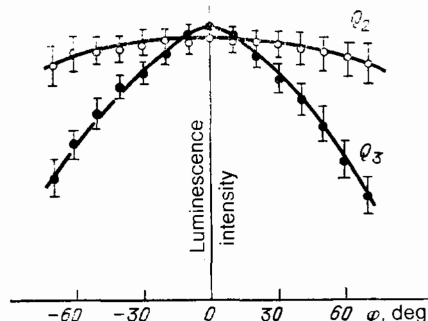

FIG. 12. Angular distribution of the luminescence intensity plotted for the Q_2 and Q_3 bands.

charge region had been observed not only for many SEI systems,[36,40,42] but also for entirely solid systems.[36,49,50] The quenching effect is usually explained as follows: an increase in a high depletion-type band bending reduces the transit time of nonequilibrium carriers crossing the space-charge layer so that it becomes increasingly shorter than the radiative lifetime. This reduces strongly the radiative recombination rate in the space-charge layer in accordance with the expression $I \propto \exp(-\alpha' d^*)$, whereas d^* is proportional to $(V - \varphi_{fb})^{1/2}$. Here, d^* is the thickness of what is known as the "dead" layer. The experiments indicate that $\ln I$ depends on $(V - \varphi_{fb})^{1/2}$.

Another mechanism which may be responsible for the photoluminescence quenching is the change in the surface recombination rate with the band bending. At present there is a tendency to analyze the photoluminescence spectra together with the Riemann spectra and with the results obtained by scanning Auger electron spectroscopy,[38,41] and to combine them with studies of the size effects influencing the photoluminescence at the interface between a variable-gap semiconductor and an electrolyte, and the deformation of the spectral profiles of impurity photoluminescence bands in the field of the space-charge region.[34,43]

7. REFLECTION AND ELECTROREFLECTION OF LIGHT AT THE SEMICONDUCTOR–ELECTROLYTE INTERFACE

The use of the SEI provides an opportunity for continuous variation of the surface potential in a wide range so that the experimentally determined dependences of the reflection and electroreflection coefficients on the electrode potential can be used to find the field intensity at the surface, the flat-band potential, as well as the energy distribution, population, and density of the surface states, to detect pinning of the Fermi level, etc., and additionally to determine such fundamental characteristics of semiconductors as the width of the band gap E_g, the exciton energy, the spin–orbit splitting, etc.[38,51,58] For example, at voltages close to the flat-band potential there is a change in the sign and a steep fall of the electroreflection signal. This has been confirmed by independent determinations of the C^{-2}–V characteristics.[55,58]

The main principles of investigation of semiconductors by electro-optic methods are described systematically in, for example, Refs. 51 and 52, but these methods are outside the scope of the present paper. Very frequently complex electroreflection spectra are recorded in inhomogeneous fields (particularly in the range of energies less than E_g) and are difficult to interpret, so that the most informative and effective approach is to combine in one investigation various optical (including modulation spectroscopic) methods with capacitance, photocapacitance, impedance, and other techniques.

By way of example we shall give below the results of an analysis of the spectra of the ZnO–electrolyte system.[30,31,45–47,59–62] Typical reflection spectra of the (1010) face of ZnO single crystals obtained at different potentials are shown in Fig. 14. The sharp peaks represent the exciton optical transitions: in the $\mathbf{E} \perp \mathbf{c}$ case a peak at 3.306 eV represents a zero-phonon transition of an A exciton, whereas in the $\mathbf{E} \parallel \mathbf{c}$ case a peak at 3.345 eV is a zero-phonon transition of a C exciton. The difference between the energies of these peaks (~ 40 meV) is due to the splitting of the valence band by the hexagonal field of the crystal lattice of ZnO. At potentials close to the flat-band value the high-energy parts of the reflection spectra exhibit an inflection separated from the energy position of the zero-phonon transitions by an amount corresponding to the energy of an LO phonon in ZnO. We can assume that the bands at 3.38 eV ($\mathbf{E} \perp \mathbf{c}$) and 3.42 eV ($\mathbf{E} \parallel \mathbf{c}$) are due to exciton transitions accompanied by the emission of one LO phonon.

An increase in the concentration N of electrically active centers increases the possibility of ionization of bulk exci-

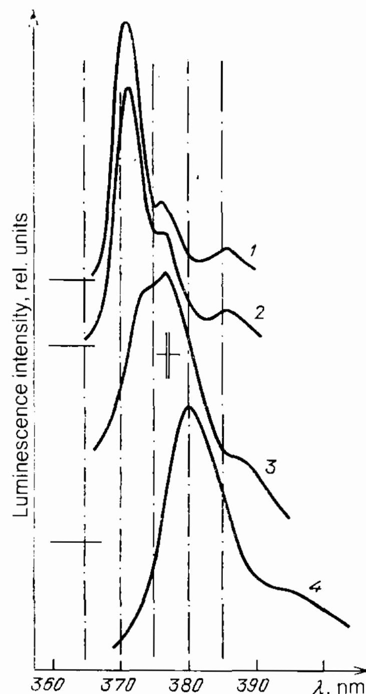

FIG. 13. Photoluminescence spectra of polycrystalline ZnO at different temperatures T (K): 1) 78; 2) 95; 3) 200; 4) 300.

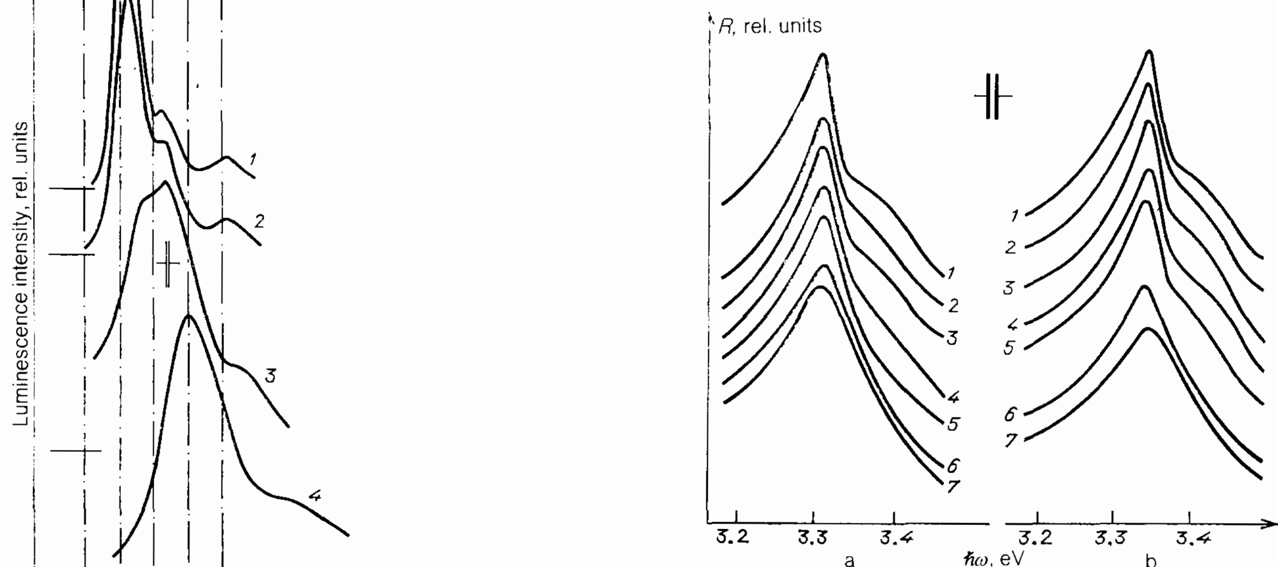

FIG. 14. Reflection spectra of the interface between a ZnO single crystal and a 0.1-N NaOH solution ($N_D - N_A \approx 10^{16}$–$10^{17}$ cm^{-3}) obtained for the $\mathbf{E} \perp \mathbf{c}$ (a) and $\mathbf{E} \parallel \mathbf{c}$ (b) polarizations subject to the following static bias voltages (V): 1) −1; 2) 0; 3) 4; 4) 8; 5) 16; 6) 32; 7) 40.

tons under the influence of a random field surrounding a defect. The critical field necessary to dissociate excitons is[63]:

$$E_{cr} = A \frac{Ze}{\varepsilon} \left(\frac{N}{r} \right)^{1/2}, \quad (7.1)$$

where ε is the permittivity; Ze is the charge of one ion; A is a constant factor (~ 2); r is the Bohr radius of an exciton. On the other hand, this critical field should obey $E_{cr} \approx \mathscr{E}_{ex}/er_{ex}$ where $\mathscr{E}_{ex}$ is the binding energy of an exciton. It therefore follows that the concentration N at which excitons in ZnO become ionized is of the order of 10^{18} cm^{-3}. At these values of N the reflection spectra become greatly modified. This is manifested most clearly by samples with a freshly cleaved surface.

An increase of the potential on the surface of ZnO gives rise to bands $K_\perp$ and $K_\parallel$ in the spectra, which shift toward lower energies and finally merge with the background (Fig. 15). A further increase in the surface potential creates new bands $L_\perp$ and $L_\parallel$ at energies $< E_g$ (ZnO) and shifts $K_\perp$ and $K_\parallel$ parallel to one another toward longer wavelengths. This is followed by the appearance of bands $M_\perp$ and $M_\parallel$, $N_\parallel$, and so on. We can see that the bands identified by the subscripts $\parallel$ and $\perp$ are separated by 40 meV and that these bands shift in parallel for both polarizations of light throughout the investigated range of bias voltages. These features are retained largely also by samples of ZnO with higher dopant concentrations.

These results taken as a whole can be explained by assuming a mechanism of formation of surface excitons associated with two-dimensional surface subbands on the assumption that only holes occupy a two-dimensional surface subband, whereas electrons are in the bulk conduction band. Their coupling to the surface is of the Coulomb nature. In the case of ZnO it has been shown experimentally that a surface subband with a high density of states does exist.

Continuous variation of the surface potential alters the energy positions of such subbands and also the number of these subbands in the band gap. This is the reason for the appearance of the K, L, M, etc. reflection bands. The density of the surface states decreases when such a subband crosses the edge of the bulk valence band and enters the band gap. Therefore, the maxima of the intensities of the K and L reflection bands are located at energies corresponding to crossing of the edge of a bulk energy band by the edge of a two-dimensional subband. The energy separation from this point to the maximum exceeds the binding energy of surface excitons (~ 100 and 60 meV for the K and L reflection bands).

The appearance of surface excitons deforms greatly the electroreflection spectra of ZnO: the long-wavelength structure shifts on increase in the bias voltage toward lower energies and oscillations appear in the short-wavelength part of the spectrum. Figure 16 shows how the amplitude of the electroreflection signal is affected by a bias voltage applied to a ZnO single crystal in the case of two different polarizations (**E**⊥**c**, Fig. 16a; **E**‖**c**, Fig. 16b); the effects at different wavelengths of the incident light are demonstrated there. The closer the photon energy is to E_g, the clearer are the oscillations. In the case of polycrystalline samples the spectra are less distinct, but the same relationships still apply. In the case of polycrystalline samples, we can expect not only bound two-dimensional surface excitons, but also tight-binding surface excitons due to image forces resulting from the formation of different phases (semiconductor, semimetal, metal) on the surface of ZnO. Surface excitons are manifested by new oscillations of the electroreflection spectra.

In the range of energies well below E_g we can use a combined method of determination of the electroreflection spectra and of the frequency dependence of the impedance of a photoelectrode[38,57,58] to determine the energy distribution of the surface states. This approach has been applied to pho-

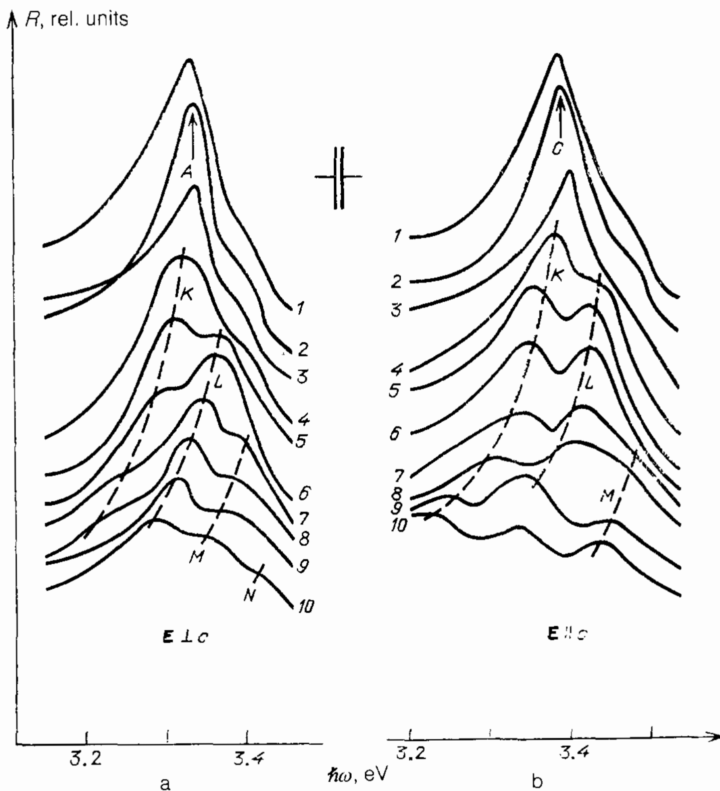

FIG. 15. Reflection spectra of the interface between a ZnO single crystal and a 0.1-N NaOH solution ($N_D - N_A \approx 10^{18}$ cm^{-3}) subjected to the following bias voltages (V): 1) -1; 2) -0.5; 3) 0; 4) 1; 5) 2; 6) 3; 7) 6; 8) 8; 9) 12; 10) 16. The dashed curves represent the shifts of the K, L, and M bands.

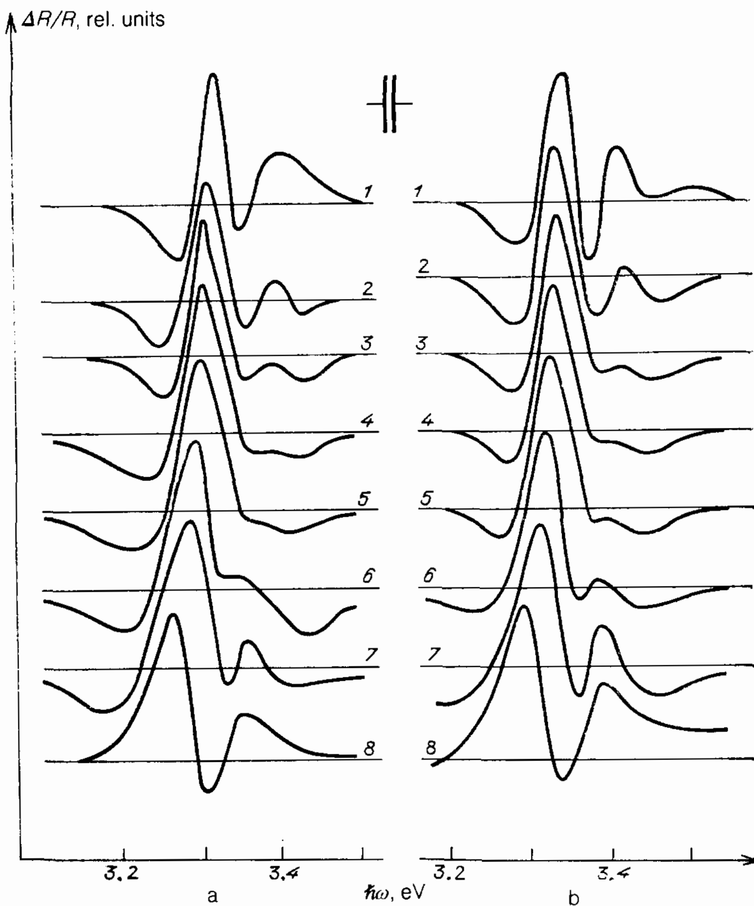

FIG. 16. Electroreflection spectra of the interface between a ZnO single crystal and a 0.1-N NaOH solution ($N_D - N_A \approx 10^{18}$ cm^{-3}) obtained for the $\mathbf{E}\perp\mathbf{c}$ (a) and $\mathbf{E}\|\mathbf{c}$ (b) polarizations under an alternating voltage of $V \sim 0.25$ volts and in the presence of static bias voltages (V): 1) −0.5; 2) 0; 3) 0.25; 4) 0.5; 5) 0.8; 6) 1.6; 7) 2.4; 8) 4.

toelectrodes made of $CuInSe_2$ and $CuIn_2Se_4$ (Refs. 58 and 57), CdSe (Refs. 53 and 54), TiO_2 (Ref. 56), and polyacetylene (Ref. 64). It would be of interest to determine also the conditions for pinning of the Fermi level by the surface states.

The electroreflection spectra obtained in weak fields are described in Refs. 38, 57, and 58 by a function

$$\frac{\Delta R}{R} = E_{\rm scr}\,(\Omega_{\rm m})\,L\,(\hbar\omega), \tag{7.2}$$

where

$$L\,(\hbar\omega) = \mathrm{Re}\,[C^* e^{i\theta}\,(\hbar\omega - E_g + i\Gamma)^{-n}]; \tag{7.3}$$

$E_{\rm SCR}\,(\Omega_m)$ field in the space-charge region modulated at a frequency Ω_m; C^* and θ are the values of the factors occurring in the amplitude and phase of the signal; $n \geqslant 2$ represents critical points for simple parabolic models, where $n = 3$ corresponds to a two-dimensional model, $n = 5/2$ applies to a three-dimensional model, and $n = 2$ represents excitons. Selection of the values of n, E_g, θ, and of the coefficient Γ representing a certain parameter can be used to describe the electroreflection spectrum. For example, the electroreflection spectrum of the $CdIn_2Se_4$–electrolyte system is described in Ref. 57 using the following parameters: $n = 2.5$, $E_g = 1.825$ eV, $\theta = 315.5°$, and $\Gamma = 0.316$. It is shown in Refs. 38, 57, and 58 that in the case of a totally depleted layer we can rewrite Eq. (7.2) in the form

$$\frac{\Delta R\,(\Omega_{\rm m})}{R} = -\frac{2eN_{\rm D}}{\varepsilon}\,L\,(\hbar\omega)\left(1 - \frac{e}{C_{\rm H}}\,\frac{{\rm d}N_{ss}^{+}}{{\rm d}U}\right){\rm d}U, \tag{7.4}$$

where C_H is the capacitance of the Helmholtz layer; N_{ss} is the density of the ionized surface states; dU is the amplitude of modulation of the electrode potential.

Equation (7.4) yields the condition

$$e\,{\rm d}N_{ss}^{+} = C_{\rm H}\,{\rm d}U, \tag{7.5}$$

which ensures that the Fermi level is pinned completely by the surface states. Since changes in the voltage drop across the Helmholtz layer result in changes in the flat-band potential $\varphi_{\rm fb}$, it follows from Ref. 57 that the latter potential can be found from

$$\varphi_{\rm fb} = \varphi_{\rm fb}^{0} + \int_{U_{\max}}^{U} \frac{e}{C_{\rm H}}\,\frac{{\rm d}N_{ss}^{+}}{{\rm d}U}\,{\rm d}U; \tag{7.6}$$

here, $U_{\max}$ is the potential at which $\Delta R/R$ passes through a maximum.

The spectral dependence of the photocapacitance of a ZnO electrode also demonstrates that the maximum of this photocapacitance occurs at energies $< E_g$ and is due to exciton absorption and field dissociation of excitons. The long-wavelength photocapacitance "tails" are clearly due to optical absorption and charge exchange.

Nonlinear optical electroreflection, representing the change in the reflection of the second harmonic in an electric field, is used in Ref. 65 as the basis of a nonlinear optical method for the investigation of semiconductor surfaces. The intensity of the reflected second harmonic is governed in particular by the lifting of the centrosymmetric forbiddenness of the dipole susceptibility near the surface, by the pres-

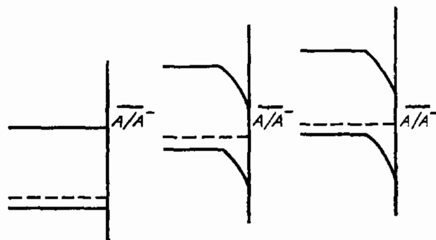

FIG. 17. Energy diagrams showing the shifts of the edges of the energy bands of a semiconductor relative to the redox potential of an electrolyte due to an increase in the illumination intensity. The diagram on the left shows the situation in the absence of illumination, the one in the center corresponds to moderate illumination, and that on the right represents the case of strong illumination.

ence of a high gradient of the normal component of the electric field vector of the pump radiation in the surface layer, and by the appearance of a high static electric field at the SEI. In particular, the proposed method was used in Ref. 65 to study the adsorption of organic molecules on the surfaces of Ge and Si, and it was found that the sensitivity of the method was sufficient to investigate not only dyes, but also molecules with much weaker nonlinear polarizabilities. Clearly, this nonlinear optical method is capable of monitoring the flat-band potential, the magnitude of the built-in charge in the oxide, and the degree of roughness of the surface and other parameters.

8. ENERGY BANDS NOT PINNED AT THE SEMICONDUCTOR-ELECTROLYTE INTERFACE

Experiments on photocathodes made of p-type Si in nonaqueous electrolytes[66–68] demonstrated the possibility of chemical reduction of a redox group with the potential significantly above the bottom of the conduction band in darkness. For example, a p-type Si photocathode was used to reduce chemically the redox group of a dimethoxynitrobenzene in methyl alcohol and of anthraquinone in acetonitrile. In darkness these redox pairs were located at 0.1 and 0.24 meV, respectively, above the bottom of the conduction band.

The distribution of the applied voltage in the region of the SEI was discussed above on the assumption that the voltage drop across the Helmholtz layer is practically constant and the applied voltage drops mainly across the space-charge region in the semiconductor and thus alters the band bending in the latter. Photoelectrons usually become thermalized in the conduction band and are injected into the electrolyte with energies corresponding to the bottom of the conduction band. Therefore, if we adopt the above ideas and ignore the heating of electrons, we find it difficult to account for reduction of the redox group level located above the bottom of the conduction band. Possible participation of hot electrons in such photoelectrochemical processes will be discussed later. Experiments carried out on Si, GaAs, and molybdenum chalcogenides[66–69] have demonstrated that the energy bands of the semiconductor are no longer pinned to any specific potentials in the presence of illumination. The changes in the voltage are then followed by the voltage drop across the Helmholtz layer and the edges of the semiconductor energy bands move upward as shown in Fig. 17, which demonstrates the shift of the energy bands relative to the redox potential A/A_- in the electrolyte as a function of the illumination intensity. The right-hand part of Fig. 17; corresponds to strong illumination, whereas the left-hand side represents the conditions in darkness and the middle part corresponds to moderate illumination of the photocathode. Photocarriers thus participate in recovery of the redox potential A/A_-. The capacitance-voltage characteristics of such a system and the nature of their changes with the intensity and frequency of illumination are similar to the characteristics of conventional MIS structures[68,70] with an inversion layer. Hence, we may conclude that the band bending in the semiconductor at the SEI should be so strong that the type of conduction is inverted and the Fermi level on the surface is closer to the valence band. A large charge then accumulates in the space-charge region of the semiconductor and the capacitance of this region becomes comparable with the Helmholtz layer capacitance, resulting in a redistribution of the voltage drops across these layers (described above) and in a shift of the edges of the semiconductor band along the energy axis.

Another possible interpretation of unpinned energy bands is proposed in Ref. 70. This effect is attributed to pinning of the Fermi level by the surface states at the SEI. The system becomes equivalent to a Schottky barrier connected in series with the electrolyte when the band edges shift with the potential applied to the SEI and the band bending in the semiconductor is not affected. In this model the process in question should be independent of the redox pairs in the electrolyte. However, the experimental results reported in Refs. 69 and 70 have shown that this is true only in the case of certain critical values of the redox potentials, so that in reality the Fermi level is not always pinned. It is therefore more likely that the pinning of the energy bands of the semiconductor at the SEI is due to the formation of an inversion layer at the semiconductor surface.

9. INJECTION OF HOT CARRIERS INTO THE ELECTROLYTE

The minority carriers created in the surface layer as a result of illumination of the semiconductor are accelerated by the electric field of the space-charge region and injected into the electrolyte. As a result of their interaction with

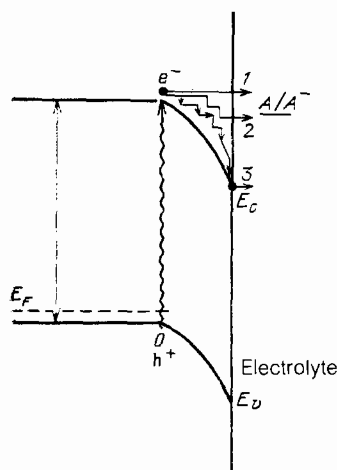

FIG. 18. Injection of hot electrons from a semiconductor into an electrolyte: 1) without thermalization; 2) with partial thermalization. Injection of thermalized electrons in equilibrium with the crystal lattice into an electrolyte is represented by curve 3.

phonons they lose their energy (become thermalized), so that at the moment of injection they are in thermal equilibrium with the crystal lattice. However, we can envisage a case when because of quantization of the energy spectrum in the surface layer of the semiconductor (see below) the photocarriers are no longer capable of transferring their energy to the lattice and are injected into the electrolyte. The likely processes are illustrated in Fig. 18. Here, cases 1 and 2 can be interpreted as injection into the electrolyte of hot electrons which are not in thermal equilibrium with the lattice.[67,70–73]

The injection of hot photocarriers into the electrolyte naturally occurs if the thermalization time of these carriers τ_{th} exceeds the sum of the times taken by these carriers to diffuse from the point of generation in the semiconductor to the SEI (τ_D), the time for the tunneling across the SEI (τ_t), and the time of relaxation in the electrolyte (τ_r). As pointed out earlier, τ_{th} increases considerably (by two orders of magnitude in the specific case discussed in Sec. 10) in the case of quantization of the energy spectrum in the surface layer of the semiconductor with a small effective mass of the minority carriers, which is due to the much higher values of the carrier energy than the phonon energy. Estimates of the times τ_D, τ_t, and τ_r obtained in Refs. 70 and 72 show that the injection of hot photocarriers into the electrolyte is possible from a heavily doped photoelectrode with small dimensions of the depletion layer. Irreversible constant-energy tunneling of photocarriers into the electrolyte implies not only fast (compared with the thermalization time) penetration of the SEI barrier, but also equally fast relaxation in the electrolyte as a result of a transition of a molecule to a new solvation state (a solvated electron can be compared in a sense to a low-mobility polaron).

Experimental investigations of the injection of hot electrons into the electrolyte should be carefully distinguished from studies of the effects which occur at the SEI when the unpinned bands are shifted along the energy axis (Sec. 8), which is investigated by recording the capacitance-voltage characteristics. Experimental proof of the injection of hot photoelectrons into nonaqueous electrolytes from p-type GaP and p-type InP is reported in Refs. 74 and 75.

Studies of the possibility of heating of photocarriers at the SEI and of their injection into the electrolyte are not only of academic interest. These studies provide an opportunity for using hot photocarriers in catalytic reactions involving redox potentials located (on the energy scale) outside the band gap of the semiconductor in darkness (for example, the reactions of binding of nitrogen to form ammonia). It is shown theoretically in Ref. 76 that photoelectrochemical conversion of the solar radiation energy is possible with the aid of hot carriers and the process can have an efficiency of 66% (under the AM1.5 conditions at 300 K). These photoelectrochemical reactions involving hot electrons probably suppress strongly the role of some surface states.

10. QUANTUM SIZE EFFECTS IN THE SURFACE LAYER OF THE SEMICONDUCTOR

If the thickness of the space-charge region in the semiconductor at the SEI is comparable with the de Broglie wavelength, quantum size effects may be expected in this region. Their main special feature is the appearance, in the allowed energy bands of the semiconductor, of a set of levels

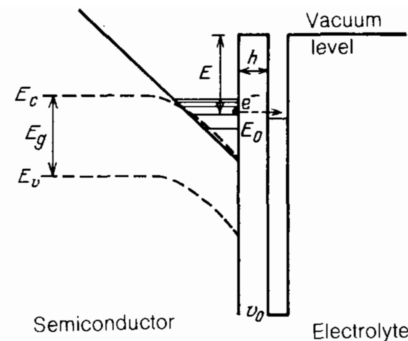

FIG 19. Model of a semiconductor–electrolyte junction.

(or two-dimensional subbands) separated by forbidden energy intervals (Fig. 19). It is known that the discrete nature of the energy spectrum results in changes in the statistics and mechanisms of carrier scattering, there are changes in the nature of their interaction with the surface states, etc. If the semiconductor surface is parallel to the crystallographic planes with high Miller indices, oriented surface superlattices may appear and these may induce further changes in the quantized energy spectrum: they may lift the degeneracy, alter the dispersion law, etc. The conditions for the appearance of the quantum size effects in surface layers of semiconductors and in thin films have been discussed extensively in the literature (see, for example, Refs. 77–79). An ion which acquires an electron from the semiconductor can be regarded as a rectangular potential well (Fig. 19).[67,70,72] The width of the well is of the order of the molecular dimensions and the depth is the same as in the semiconductor. The well is located at a distance h from the surface. We shall assume that on the semiconductor side there is an asymmetric potential well, which is bounded on one side by the parabolic potential of a depletion layer of height equal to the potential representing the band bending, whereas on the other side there is a very high vertical wall formed by the barrier between the semiconductor and the electrolyte. If the SEI is regarded as a heterojunction, then the height of this barrier represents the difference between the "bottom of the conduction band" of water and the energy of the conduction band of the semiconductor.

Simultaneous solution of the one-dimensional Schrödinger equation and the one-dimensional Poisson equation for such an asymmetric potential well is possible only by numerical methods. Analytic expressions can be obtained employing a simpler model of the parabolic potential of a depletion layer approximated by a linear dependence of the band bending on the coordinate. This triangular shape of the well makes it possible to separate the variables and to obtain the exact solutions of the Schrödinger equation. The wave functions of carriers in a triangular well are Airy functions $\Phi(\xi)$ and the energy of the mth level can be described by the expression

$$E_m = \left[\frac{3\pi\hbar e F_s}{(8m^*)^{1/2}}\left(m+\frac{3}{4}\right)\right]^{2/3}, \qquad (10.1)$$

where F_s is the direction of the electric field at the surface. The effective mass approximation is also used here.

It follows from Eq. (10.1) that under quantization conditions the first discrete level ($m=0$) no longer coincides

with the bottom of the conduction band, but lies above it and is separated by

$$E_0 = \left[\frac{9\pi e \hbar F_s}{8 (2m^*)^{1/2}} \right]^{2/3}. \tag{10.2}$$

An increase in the quantum number m reduces the separation between the discrete levels and the spectrum may gradually become quasicontinuous. The scattering of carriers and other factors can broaden the levels, but even when all the upper levels overlap completely, the spectrum is still separated from the bottom of the conduction band by the energy E_0. The effective rate of surface recombination and the separation between E_0 and the surface states change under quantization conditions.[50]

In high surface fields F_s the surface well may contain just the lowest level at room temperature. If $E_1 - E_0 \gg kT$, then this case is referred to as the quantum limit. It applies to many semiconductors at $T = 300$ K.

Estimates obtained for a triangular well of height 1 eV show[70,72] that if $m_p^* = 0.01 m_0$, the well contains just one energy level separated by 0.56 eV from the bottom of the well. Obviously, for this energy spectrum the thermalization time of carriers increases considerably because the process of thermalization involves multiphonon scattering and this is a slower process than one-phonon scattering. Estimates given in Ref. 70 indicate that the thermalization time τ_{th} is of the order of 10^{-11} s even for $E_0 \approx 0.1$ eV, in contrast to 10^{-13} s in the case of one-phonon energy dissociation. The larger the effective mass, the greater the interval between the energy levels and the higher the value of the energy E_0 [see Eqs. (10.1) and (10.2)], the higher the probability of one-phonon dissociation, and the shorter the thermalization time of carriers.

11. SUPERLATTICE PHOTOELECTRODES

The phenomena occurring in arrays of quantum wells coupled quantum-mechanically are currently attracting very great interest. Structures composed of such wells are known as superlattices (see, for example, Ref. 80).[5)]

The first reports of investigations of photoelectrodes based on a 40-layer $GaAs$–$GaAs_{0.5}P_{0.5}$ superlattice were published by A. J. Nozik *et al.*[81,82] The quantum size effects were observed in GaAs ($E_g = 1.42$ eV) quantum wells of thickness 250 Å or 50 Å and the thickness of the $GaAs_{0.5}P_{0.5}$ ($E_g = 2.0$ eV) barriers was 250 Å. Figure 20a shows the energy diagram of such a structure and it gives the energies of allowed ($\Delta n = 0$) transitions 1–6 and of a forbidden ($\Delta n = 1$) transition 6′. The substrate in these structures was a plate of p^+-type GaAs and the ohmic contact was made of gold. A buffer layer of $GaAs_{1-x}P_x$ with $x = 0$–0.25 was formed between the superlattice and the substrate: this layer consisted of five identical sublayers (2-μm thick), but with values of x increasing away from the substrate. The top sublayer of the photoelectrode consisted of GaAs. The height of the electron barrier in the conduction band was 0.28 eV and the height of the hole barrier in the valence band was 0.30 eV.

The photoelectrode was immersed in solutions of 0.2 M ferricyanide dissolved in 1 M H_2SO_4 or solutions of 0.1 M Eu^{3+} dissolved in 1 M $HClO_4$. The wavelength dependences of the quantum efficiency of the photoelectrode (Fig.

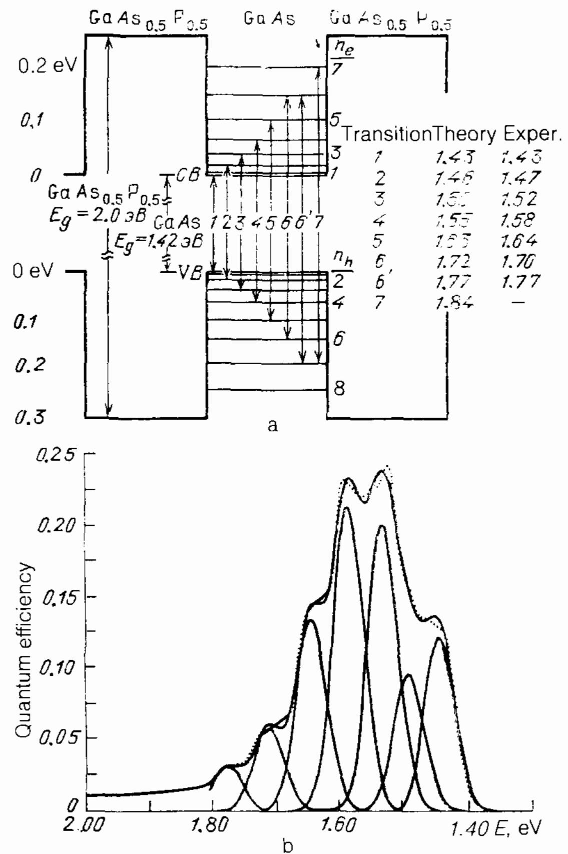

FIG. 20. Transitions in a $GaAs/GaAs_{0.5}P_{0.5}$ superlattice (a) and the spectral dependence of its quantum efficiency (b).

20b) indicated that the room-temperature data for the superlattice photoelectrode were in excellent agreement with the overall envelope of seven Gaussian curves plotted for the first six allowed transitions ($\Delta n = 0$). The seventh experimentally observed peak represented the forbidden ($\Delta n = 1$) transition 6′ shown in Fig. 20a.

It is worth noting the considerable broadening of the photocurrent spectrum in the direction of higher energies and a significant increase (doubling to 32%) of the quantum efficiency of the superlattice with the GaAsP barrier thickness 50 Å compared with the superlattice with the barrier thickness 250 Å. It should be stressed that a significant quantum efficiency (in excess of 4%) was observed in a fairly narrow range of wavelengths (~50–70 nm between 0.81 and 0.83 μm), whereas the quantum efficiency for the p-type GaAs film was 70% at 0.825 μm. Moreover, it was found that the quantum efficiences were higher, compared with Eu^{3+}, when use was made of $Fe(CN)_6^{3-}$ acceptors, i.e., the observed photocurrents depended—as expected—not only on the intensity of illumination of the photoelectrode, but also on the laws governing the transport of carriers in the photoelectrode.

A characteristic feature of the photocurrent spectrum obtained for the superlattice system was reversal of the sign of the photocurrent. For example, the sign was reversed at 775 nm in the case of zero bias on the photoelectrode. Under negative bias voltages (relative to a saturated calomel electrode) the transport of electrons took place from electron states in the quantum well to the electrolyte, giving rise to a

cathodic photocurrent. Most likely this transport occurred from all the states except for the lowest ($n_c = 1$). At positive bias voltages the photocurrent was of anodic nature and was a consequence of the transport of holes from the hole wells (Fig. 20a). The competition between these two types of carrier caused the reversal of the sign of the photocurrent at certain values of the electrode potential. It was concluded in Ref. 82 that the results provided a convincing experimental proof of partial thermalization of electrons and of active participation in the observed processes of hot electrons injected into the electrolyte from the high-energy states in the electron quantum well in the semiconductor. The absence of the theoretically predicted exciton peaks in the photocurrent spectrum, the nature of its dependence on the photon energy, and the mechanisms of carrier transport within the superlattice electrode would require further analysis.

An investigation of $GaAs-Al_{0.38}Ga_{0.62}As$ superlattice electrodes was also reported in Ref. 83.

12. QUANTUM SIZE EFFECTS IN SEMICONDUCTOR COLLOIDS

The quantum and size effects in three dimensions occur in semiconductor microcrystals (crystallites) immersed in an electrolyte. Experimental studies have been made of colloids (see, for example, Ref. 7) based on microcrystals of CdS, PbS, ZnS, HgSe, PbSe, and CdSe (with crystallite diameters from 20 to 200 Å).[84–86] Calculations have also been made for InSb, GaAs, and ZnO crystallites in a liquid "matrix."[87] A microcrystal is essentially a three-dimensional potential well, the dimensions of which limit free motion of quasiparticles, so that their energy spectra are quantized.

It is most probable that reduction in the linear size of crystallites creates discrete electron states in the conduction and valence bands (as shown in Fig. 20a) and these states then participate actively in photoelectrochemical processes. The "effective" width of the band gap of microcrystals increases and the work function for the emission of electrons decreases. "The quantum size effects are manifested most strongly in semiconductors with a small effective mass of carriers (primarily electrons) because in the first approximation the energy of the quantum states is inversely proportional to the effective mass and to the square of the linear size of a microcrystal (in a simplified theoretical treatment a crystallite is regarded as a sphere). Calculated dependences of the energy of the lowest electron state in the conduction band on the crystal diameter are given in Fig. 21 (Ref. 87).

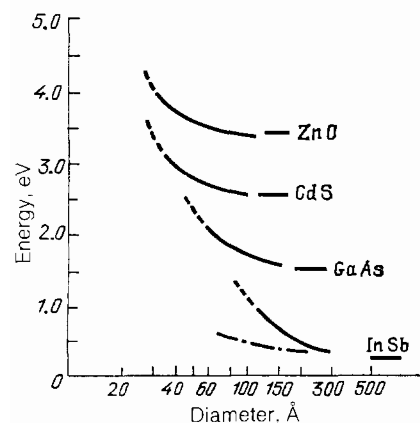

FIG. 21. Dependence of the energy of the lower energy state on the diameter of crystallites. The horizontal line shows the width of the band gap of the investigated semiconductors.

The problem of the quantum size effects in the spectra of the exciton and interband absorption by spherical microcrystals is discussed in Ref. 88. A detailed theoretical study of the size quantization of excitons is reported in Ref. 89 for the specific case of CuCl single crystals grown in a silicate glass matrix. An analysis is made there of the position and profile of the exciton absorption and luminescence lines on the size of microcrystals. The calculated dependences agree with the experimental results.[89,90] The approach and the model proposed in these investigations can be developed further in the case of colloids.

Experimental studies[85,86] of CdS, CdSe, PbS, PbSe, and HgSe colloids have shown that reduction of the crystallite size shifts considerably the fundamental absorption edge toward shorter wavelengths (blue shift) and this represents an effective increase in the width of the band gap. For example, in the case of HgSe with $E_g = 0.35$ eV the absorption edge for crystallites of 20–30 Å size shifts by 2.8 eV; in the case of CdS crystallites of < 50 Å size the shift is 0.9 eV and in the case of PbS ($E_g = 0.4$ eV) the shift amounts to ~ 2 eV for crystallites of ~ 20–30 Å size and ~ 1 eV for 50–200 Å. It is interesting that in the case of CdS microcrystals in an insulating matrix the shift is ~ 0.8 eV (Ref. 91). The photoluminescence spectra of semiconductor colloids have "unusual" maxima (at 430 nm for HgSe, 360 nm for CdS, and 430–600 nm for PbS), which are again attributed to an increase in the energy gap.

Injection of hot electrons into an electrolyte containing microcrystals makes it possible to realize the photoelectrochemical reactions mentioned in Sec. 9 which are impossible in the case of bulk photoelectrodes. For example, it is demonstrated in Ref. 86 that hydrogen can be generated using 50 Å PbSe and HgSe colloids and CO_2 can be reduced by 50 Å CdSe colloids, whereas in the case of bulk electrodes made of the same semiconductors these reactions cannot be realized.

13. CLASSIFICATION OF PHOTOELECTROCHEMICAL CELLS

When two photoelectrodes placed in an electrolyte are illuminated, we can expect the same reaction in the forward and reverse directions or two different reactions. In the former case the Gibbs energy G in the electrolyte is constant: cells of this kind are used for the conversion of the optical into electrical energy and they are known as regenerative or "liquid" solar cells. If $\Delta G \neq 0$, as in the case when the reactions on the cathode and anode are different and not reversible, the cells characterized by this inequality are used in photosynthesis and for photoelectrochemical reactions stimulated by the energy of the incident light. In the case of energy-releasing ($\Delta G > 0$) reactions the chemical energy accumulates in the system (for example, photodissociation of water results in the accumulation of hydrogen and oxygen). In photocatalysis, when energy-consuming reactions are activated (for example, when ammonia NH_3 is synthesized from N_2 and H_2) the optical energy is used in reactions in which an activation barrier has to be overcome (practically impossible in darkness).

We shall now consider briefly the processes occurring in such cells and we shall begin with photodissociation (pho-

TABLE I. Efficiencies of regenerative photoelectrochemical cells.

Electrode	Efficiency, %	Illumination conditions
1. Aqueous electrolytes:		
n-CdSe		
single crystal (sc) (M K)	12.4	AM2
thin film (tf)	7	AM1
n-$CdSe_{0.65}Te_{0.35}$		
sc	12.7	—
tf	8	—
n-CdTe sc	10.0	AM1
n-GaAs		
sc + Ru	12	AM1
sc + polymer	12	AM1
tf	7.3	AM1
n-ZnSe sc	10.4	366 nm
n-$MoSe_2$ sc	9.4	AM1
n-MoS_2 sc	9.8—13.4	633 nm
n-$GaAs_{0.72}P_{0.28}$ sc	11	AM2
»	30	633 nm
n-$GaAs_{0.6}P_{0.4}$ on GaAs substrate		
tf	16	458 nm
p-InP sc	11.5	633 nm
n-WSe_2 sc	14	590 nm
p-WSe_2 sc	10.2	AM1
$CuInSe_2$ polycrystalline (pc)	12	100 mW/cm^2 (Xe lamp)
» » »	10	AM1
tf	5.9	AM1
2. Heteroelectrodes and complex electrodes:		
Tl_3O_2 — n-Si	11	75.3 W/cm^2 (sun)
ditto.	13.8	80 mW/cm^2 (Xe lamp)
» »	14.6	15 mW/cm^2 (Xe lamp)
Tl_2O_3 — n-Si	22.3	15 mW/cm^2 ($\lambda = 800$ nm)
GdSe — p^+/n-Si	9	AM2
Pt — p^+/n-Si	7.1—9.8	AM1
W — p^+/n-Si	7.0—8.1	AM1
Mo — p^+ n-Si	7.0—8.1	AM1
Pt — MgO⟨Li⟩ — n-Si	13	AM1
Pd/Cr — SiO_x — p-Si	6.1	AM1
Pt — SiO_2 — n-Si	8—8.6	AM1
3. Nonaqueous electrolytes:		
n-GaAs		
sc	15.1	5.3 mW/cm^2 (Xe lamp)
pc	4.8	—
n-$GaAs_{0.72}P_{0.28}$	13.2	—
CdS	9.5	—
n-Si sc	14	100 mW/cm^2 (halogen lamp)
n-Si sc	12	AM2
p-Si sc	10.5	—
a-Si : H tf	4.2	8.3 mW/cm^2

tolysis) of water. This reaction can occur in a photoelectrochemical cell consisting of a solid anode and a solid cathode forming a capacitor containing an aqueous electrolyte.[93] Molecular oxygen is released in the gaseous form at the anode and molecular hydrogen at the cathode. The products of photolysis accumulate at the electrodes which are separated in space. When these electrodes are connected to an external emf source, the process is called photoelectrolysis of water.

The main materials used as photocathodes in photoelectrochemical cells are currently semiconductor oxides TiO_2, $SrTiO_3$, ZnO, and Fe_2O_3, the main advantage of which is photocorrosion resistance under high anodic potentials.

Summaries of information on these and other numerous materials used as photoanodes can be found, for example, in Refs. 2–6 and 93–95, and in the bibliography in Ref. 8. The efficiencies attained in conversion of solar energy into chemical energy (under AMl illumination conditions) range up to 1.8% for a TiO_2 photoelectrode and 1.3% for ZnO. Ceramic Fe_2O_3 electrodes are characterized by efficiencies not exceeding 1%.

The values of the efficiency of photoelectrolysis obtained for single-crystal electrodes are contradictory. For example, an efficiency of ~20% for an $SrTiO_3$ single-crystal electrode has been reported for illumination with monochromatic light of photon energy 3.8 eV. Efficiencies of 5%–8% are given in the literature for a TiO_2 electrode containing a fired-in paste of $LaCrO_3$, $LaAuO_3$, $LaRbO_3$, or $LaVO_3$, but also in this case calculations allow for the energy of a xenon lamp in the range of wavelengths from 300 to 600 nm. A photocathode consisting of a single crystal of *n*-type CdTe doped with indium is reported[33] to have an efficiency of 10% in photodissociation of an aqueous electrolyte representing a 7-N solution of $SnCl_2$. A high efficiency of photoelectrolysis of a 1-M solution of $HClO_4$ is given in Ref. 96 for a *p*-type InP photocathode (saturated with hydrogen, rhodium, or rhenium).

Photoelectrolysis of HBr and HI acids has also been achieved.[7,96,97]

The current-voltage characteristic of a "liquid" regenerative solar cell is identical with the characteristic of a solid-state cell. The best efficiencies of photoelectrochemical conversion of solar energy into electrical energy are given in Table I. In addition to the materials listed in this table there have been reports of less efficient regenerative cells utilizing a very great variety of single-crystal and polycrystalline semiconductor materials and thin semiconductor films (see, for example, Refs. 2, 4–11, and 98–108).

There have been practically no studies of aerobic (gas-filled) regenerative cells.[109] These cells operate in the presence of oxygen and hydrogen in an electrolyte; the gases are usually supplied from outside. For example, in an oxygen atmosphere there is a considerable change in the steady-state electrode potential. This change can be very considerable for some electrodes. For example, in the case of *p*-type CdTe the onset of the appearance of the photocurrent in the presence of oxygen in an electrolyte is shifted by about 0.5 V toward negative potentials.

The working life of regenerative photoelectrochemical cells is still short for extensive practical applications, although some cells have worked up to 18 months.

14. SEMICONDUCTOR HETEROELECTRODES

In the above account of the possibility of using various semiconductors in photoelectrochemical cells we have discussed simple electrodes made of one specific semiconductor. It is also possible to employ complex electrodes representing two-layer or multilayer structures differing in respect of the component materials and in respect of the type and nature of conduction. Such structures can be made of various semiconductors or semiconductor structures with *p-n* or *h-l* junctions coated by a thin metal layer.

Back in 1976–77 suggestions have been made[2,4,5,110] that photoanodes resistant to photocorrosion can be made from semiconductors with relatively narrow band gaps (Si, GaAs, InP, GaAlAs) if they are coated by a film of a stable wide-gap material with the same type of conduction (TiO_2, SnO_2, Al_2O_3, Si_3N_4, MoO_3). Heteroelectrodes have also been made utilizing isotypic *n-n* junctions of the GaAs–CdS, CdSe–Si, or CdSe–CdS type.[111] Various methods for the formation of protective coatings have been proposed. It has been found that even practically nonporous thin films can reduce considerably the photocorrosion of the narrow-gap part of a heterojunction, but cannot prevent diffusion of the electrolyte across the film to the narrow-gap semiconductor. On the other hand, very thick (>500 Å) films of a wide-gap semiconductor hinder the passage of photoholes generated by radiation in a narrow-gap semiconductor across the wide-gap layer to the SEI. Such passage of photoholes is also hindered by a considerable energy barrier ΔE_v which forms as a result of the difference between the energy positions of the valence band in the wide- and narrow-gap parts of a polytypic *n-n* heterojunction. For example, the height of the barrier hindering holes in the CdSe–CdS system observed in the case of photoelectrochemical reactions on a CdSe electrode in polysulfide solutions is approximately 0.5 eV, and a similar barrier ΔE_v is observed in the case of Fe_2O_3–Si. Such a barrier cannot be overcome by the majority of photoholes and the films are far too thick for the tunneling. Moreover, we can have a situation when the efficiency of these processes decreases compared with the case when an oxide is grown on a metal substrate. This may occur if a heterostructure has a barrier hindering electrons ΔE_c, which must affect electron transport from the SEI to the ohmic contact. This has been demonstrated, for example, in the case of an *n-n* TiO_2–Si junction and also in the case of a TiO_2 film grown on a titanium substrate.[110]

It is reported nevertheless[112–113] that a photocurrent generated by radiation absorbed in silicon is generated in Fe_2O_3–Si. This was observed for an Fe_2O_3 film of thickness of the order of 2000 Å and a relatively high—for Fe_2O_3—quantum efficiency (from a few percent to 40%) was achieved for anode potentials in excess of 0.6 V relative to a saturated calomel electrode at wavelengths 550–1140 nm. At lower potentials the photoresponse was observed only at wavelengths 250–550 nm. The spectral dependence of the photocurrent varied with the spectrum when a single crystal of silicon was replaced with amorphous hydrogenated silicon (*a*-Si:H). It was reported in Ref. 114 that a silicon electrode exhibited long-term stability (it was operated for over 650 h continuously) in photoelectrolysis of water when this electrode was coated by a thin Mn_2O_3 film: the electrode current was unaffected by operation for eight months.

The next step in the formation of electrodes on the basis of *n-n* isotypic junctions involved the use of n^+-n Si–TiO_2 and n^+-n Si–Bi_2O_3 junctions.[110] An n^+-n homojunction was used to improve the ohmic nature of the contact and prevented reverse motion of electrons from the contact.

A heterojunction between CdSe and p^+/n-Si formed by deposition of a cadmium selenide film on a cleaned and then passivated surface of a p^+-n solar cell was used in Ref. 111 in a regenerative liquid cell with a polysulfide electrolyte; its efficiency was 9%.

Series connection of two junctions (heterojunction and homojunction or two heterojunctions)[115] is one of several promising solutions. Electrodes made of an isotypic heterojunction in which an external (in contact with the electrolyte) layer was a degenerate semiconductor, in which the absorption of light could not induce any significant photocurrent, are described in Refs. 116–118. In this case only the carriers generated by long-wavelength radiation play a role in the layer protected from photocorrosion. Such photoanodes have been made from *n*-type silicon covered by a layer of degenerate SnO_2, Tl_2O_3, or a mixture of indium and tin oxides (ITO). We are dealing here in fact with a Schottky barrier. It is interesting to note that SnO_2 and ITO deposited on *n*-type silicon act as photohole "sources." Photoelectrons moving toward the SnO_2–Si interface recombine in silicon with holes generated by long-wavelength radiation in the latter material. Photoelectrons in silicon pass through a short-circuited external cell and participate in the reduction of water on a platinum counterelectrode. Here in photoanodes made of anisotypic *n*-Si–SnO_2 or Si–ITO heterojunctions both layers participate in the conversion process and the photocurrent is usually governed by the minimum rate of photogeneration of electrons and holes in any one of the layers. The potential of the Si photoelectrode is more negative than that of the ITO or SnO_2 electrodes, so that the process of photolysis of water does not require an external voltage or a difference of pH between the cathode and anode parts of a photolysis cell.[119] In the regenerative regime an electrode based on a heterojunction of the *n*-Si–SnO_2 type was found to have an efficiency of 4.8% in the presence of an $Fe(CN)_6^{4-13-}$ redox pair. In the case of *n*-type Si–Tl_2O_3 used in a regenerative liquid cell the efficiency was found to be 11% (Table I). A comparison of this cell with a solid cell with the same base indicated[117] that their characteristics were very similar and that the main role was played by the solid-state heterojunction between silicon and Tl_2O_3.

The properties of an electrode based on *n*-CdS–RuO_2 or

p-Si–RuO_2 were reported in Ref. 120. Ruthenium dioxide has a partly filled $4d$ orbital and, therefore, a high electronic conductivity, so that it can be regarded more as a metal than a degenerate semiconductor.

15. COMPLEX ELECTRODES WITH A THIN METAL FILM DEPOSITED ON A SEMICONDUCTOR

The deposition of a metal film on a semiconductor for the purpose of increasing its electrocatalytic activity is a familiar and successfully used method in electrochemistry of semiconductors. A metal is deposited either in the form of a continuous thin film so that light is transmitted across the metal–semiconductor interface or in the form of islands or spots or as a highly porous film on the surface of a semiconductor ensuring that the semiconductor is in direct contact with an electrolyte. In some cases metal silicide films have been used on the surface of silicon. The best results obtained for photoelectrodes with a thin metal film are listed in Table I (Refs. 5, 7, 97, 103–105, 117, and 121–123).

16. HETEROELECTRODES BASED ON INORGANIC AND ORGANIC SEMICONDUCTORS

Physical and chemical processes in organic semiconductors are currently attracting much attention of scientists working in different disciplines.[124–128] The most interesting n-type polymers with various potential applications are trans-$(CH)_x$ (polyacetylene), polypyrrole, polyaniline, polyparaphenylene. The main features of these polymers are the existence of systems of conjugate bonds, soliton conduction mechanism, and the ability to reach a high electrical conductivity by doping a polymer with donors or acceptors, and, consequently, the ability to establish n- or p-type conduction in these materials.

Photocurrents in photoelectrochemical cells with organic semiconductor electrodes are very low, so that such cells are of little interest as electrode materials themselves. However, they can be used as an external layer, in contact with an electrolyte, in complex heterojunctions. Such materials have already been used as protective coatings for Si, GaAs, GaP, InP, chalcogenides and dichalcogenides of various metals, and oxides TiO_2, SnO_2, and ITO in aqueous and nonaqueous solutions.

In particular, some p-type polymer semiconductors are transparent over a large part of the visible spectrum and can easily be deposited in the form of thin films resistant to photocorrosion, so that in an analysis of the processes in two-layer systems consisting of organic and inorganic semiconductors one can draw on an analogy with heterophotoelectrodes discussed above. For example, the width of the band gap E_g of polypyrrole, which is a polymer used most widely in photoelectrochemical cells, is the same as E_g for Fe_2O_3 and amounts to 2.2 eV. A nearly perfect Schottky barrier forms at the interface between polypyrrole and an inorganic semiconductor. For a cell containing an electrode coated by polypyrrole and a Pt electrode the efficiency of regenerative conversion can be quite high: when n-type GaAs is used in an aqueous solution of $[Fe(CN)_6^{4-/3-}]$ with an excess of CN^- ions the efficiency is 10.6%, whereas for n-type Si with a Pt sublayer it is 2.3–2.8% (Refs. 7, 125, 127, and 129). The efficiency of such photoconversion can be controlled in principle by deposition of noble metals on the surface of a polymer[132–133] or by introduction of particles of an electrocatalyst into the polymer: these particles may consist of Pd (Ref. 132), or of other metals belonging to the platinum group and of their oxides, such as RuO_2 (Refs. 131 and 133), etc.

In addition to organic semiconductors, protective coatings of inorganic semiconductors can be in the form of insulating ion-exchange polymers containing ions and redox particles. These polymers include polysiloxane, polyindole, polyorthophenylenecyanine, and Nafion.[110,131,134-136] Photoelectrochemical processes in such systems do not occur at the SEI, but directly at the semiconductor–polymer interface where ions (for example, H^+) that have diffused across the polymer react with the inorganic semiconductor. Films of polyvinylpyridine with $Ru(bipy)_2Cl$ (Refs. 137 and 138), polymer viologens (Refs. 132, 139–141), etc., which themselves are redox polymers, are used as protective photoelectrodes.

Common shortcomings of complex heteroelectrodes based on inorganic semiconductor–polymer structures are their poor (at least at present) stability, a short service life, a low efficiency, and inability of many to operate at normal or high solar radiation intensities. The expected advantages are the ability to operate in contact with solid electrolytes (polyethylene oxide with a KI/I_2 redox pair,[130] etc.), feasibility of constructing photoelectrochemical cells consisting entirely of solids, applications in electrochromic displays, as comparison electrodes, and as sensor systems.[110,142,143]

17. CONCLUSIONS

Efficient photoelectrodes for the transformation of radiant energy and for photocatalysis will become available as a result of interdisciplinary research involving physics of semiconductors, chemical physics, materials science, photoelectrochemistry of semiconductors, microelectronics, catalysis, semiconductor technology, etc. Such research is proceeding actively in many countries and new striking results can be expected in the near future.

The author is grateful to L. P. Pitaevskiĭ for his interest.

[1)]The International Electrochemical Society is recommending this term.

[2)]The scale of potentials used in electrochemistry is based on the assumption that the potential of a normal hydrogen electrode is zero, i.e., that $U_{NHE} = -4.44$ V.

[3)]This is discussed in greater detail in the next few paragraphs.

[4)]In contrast to the contact potential, the Galvani potential cannot be measured directly, because we are dealing here with the potential difference between points in different phases.

[5)]If such structures consist of a series of alternate n- and p-type layers, they can be called doped superlattices. The possibility of using them in photoelectrochemistry of semiconductors has not yet been discussed.

[1]S. R. Morrison (ed.), *The Chemical Physics of Surfaces*, Plenum Press, NY, 1976 [Russ. transl., Mir, M., 1980].

[2]Yu. V. Gurevich and Yu. V. Pleskov, *Photoelectrochemistry of Semiconductors* [in Russian], Nauka, M., 1983.

[3]H. Gerischer, in *Solar Energy Conversion: Solid-State Physics Aspects* (ed. by B. O. Seraphin), Springer Verlag, Berlin, 1979, p. 115 [Topics in Applied Physics, Vol. 31].

[4]V. M. Arutyunyan, *Photocatalytic Solar Energy Conversion* [in Russian], Nauka, Novosibirsk, 1985, p. 74.

[5]V. M. Arutyunyan, in: *Photodetectors and Solar Cells* [in Russian], Nauka, Leningrad, 1986, p. 253.

[6]Yu. V. Pleskov, *Physical Chemistry: Current Topics* [in Russian], Khimiya, M., 1985, p. 64.

[7]*Energy Resources Across the Prism of Photochemistry and Catalysis* [Russ. transl.], Mir, M., 1986.

[8]K. Kalyanasundaram, Sol. Cells **15**, 93 (1985).
[9]Proc. All-Union Conf. on Photocatalytic Solar Energy Conversion [in Russian], Novosibirsk, 1983.
[10]Proc. Second All-Union Conf. on Photocatalytic Solar Energy Conversion [in Russian], Leningrad, 1987.
[11]Proc. Second All-Union Conf. on Renewable Energy Sources [in Russian], Erevan, 1985.
[12]R. Memming, in Comprehensive Treatise of Electrochemistry, Vol. 7, *Kinetics and Mechanisms of Electrode Processes* (ed. by B. E. Conway, J. O'M. Bockris, E. Yaeger, S. U. M. Khan, and R. E. White), Plenum Press, N. Y., 1983, p. 529.
[13]J. S. Blakemore, *Semiconductor Statistics*, Pergamon Press, Oxford, 1962.
[14]R. H. Kingston and S. F. Neustadter, J. Appl. Phys. **26**, 718 (1955).
[15]D. R. Frankl, J. Appl. Phys. **31**, 1752 (1960); C. E. Young, J. Appl. Phys. **32**, 329 (1961).
[16]S. U. M. Khan and J. O'M. Bockris, in Comprehensive Treatise of Electrochemistry, Vol. 7, *Kinetics and Mechanisms of Electrode Processes* (ed. by B. E. Conway, J. O'M. Bockris, E. Yaeger, S. U. M. Khan, and R. E. White), Plenum Press, N. Y., 1983, p. 41.
[17]V. A. Myamlin and Yu. V. Pleskov, *Electrochemistry of Semiconductors*, Plenum Press, N. Y., 1967.
[18]Zh. R. Panosyan, V. M. Arutyunyan, A. G. Sarkisyan, *et al.*, Poverkhnost' No. 4, 147 (1983) [Phys. Chem. Mech. Surf. (1983)].
[19]Zh. R. Panosyan, V. M. Arutyunyan, A. R. Mailyan, and G. S. Bornazyan, Poverkhnost' No. 2, 93 (1986). [Phys. Chem. Mech. Surf. (1986)].
[20]F. F. Vol'kenshteĭn, *Electronic Processes on Semiconductor Surfaces Under Chemisorption Conditions* [in Russian], Nauka, M., 1987.
[21]A. V. Rzhanov, *Electronic Processes on Semiconductor Surfaces* [in Russian], Nauka, M., 1971.
[22]V. M. Arutyunyan *et al.*, Fizika (Erevan) No. 8, 156 (1987); V. M. Harutunian, A. G. Sarkissyan, and G. E. Shahnazaryan, J. Electrochem. Soc. **134**, 144C (1987).
[23]W. W. Gärtner, Phys. Rev. **116**, 84 (1959).
[24]J. I. Pankove, *Optical Processes in Semiconductors*, Prentice-Hall, Englewood Cliffs, N. J., 1971 [Russ. transl. Mir, M., 1979].
[25]T. S. Moss, G. J. Burrell, and B. Ellis, *Semiconductor Opto-Electronics*, Butterworths, London, 1973 [Russ. transl., Mir, M., 1976].
[26]V. M. Arutyunyan *et al.*, Alternative Energy Sources: Proc. Soviet–Italian Symposium [in Russian], Part 2, Énin, Moscow (1983), p. 29.
[27]A. G. Sarkisyan V. M. Arutyunyan, G. M. Stepanyan, *et al.*, Elektrokhimiya **21**, 261 (1985). [Sov. Electrochem. **21**, 238 (1985)]
[28]Zh. R. Panosyan, V. M. Arutyunyan, and G. S. Bornazyan, Electrokhimiya **21**, 846 (1985) [Sov. Electrochem. **21**, 786 (1985)].
[29]V. M. Arutyunyan *et al.*, Izv. Akad. Nauk Arm. SSSR Fiz. **20**, 96 (1985).
[30]A. L. Marg[illegible]an, Author's Abstract of Thesis for the Degree of Candidate of Physicomathematical Sciences [in Russian], Odessa (1986).
[31]A. L. Margaryan, Zh. R. Panosyan, V. M. Arutyunyan, and V. A. Meliksetyan, Fizika (Erevan) No. 8, 118 (1987); V. M. Harutunian, H. L. Margarian, V. A. Melicksetian, and J. R. Panossian, J. Phys. Condens. Matter **1**, 847 (1989).
[32]A. G. Sarkisyan *et al.*, Fizika (Erevan) No. 8, 150 (1987).
[33]Zh. R. Panosyan, V. M. Arutyunyan, and V. A. Meliksetyan, Fiz. Tekh. Poluprovodn. **19**, 1633 (1985) [Sov. Phys. Semicond. **19**, 1005 (1985)].
[34]F. R. F. Fan and A. J. Bard, J. Phys. Chem. **89**, 1232 (1985).
[35]H. H. Streckert, H. Van Ryswyk, R. N. Biagioni, and A. B. Ellis, J. Phys. Chem. **88**, 1544 (1984).
[36]P. M. Smiley, R. N. Biagioni, and A. B. Ellis, J. Electrochem. Soc. **131**, 1068 (1984).
[37]F. Decker, M. Abramovich, and P. Motisuke, J. Electrochem. Soc. **131**, 1173 (1984).
[38]M. Tomkiewicz, Proc. SPIE Int. Soc. Opt. Eng. **452**, 120 (1984).
[39]R. Garuthara, M. Tomkiewicz, and R. P. Silberstein, J. Appl. Phys. **54**, 6787 (1983).
[40]W. S. Hobson and A. B. Ellis, J. Appl. Phys. **54**, 5956 (1983).
[41]R. P. Silberstein and M. Tomkiewicz, J. Appl. Phys. **54**, 5428 (1983).
[42]F. R. F. Fan, P. Leempoel, and A. J. Bard, J. Electrochem. Soc. **130**, 1866 (1983).
[43]H. H. Streckert and A. B. Ellis, J. Phys. Chem. **86**, 4921 (1982).
[44]D. Fichou and J. Kossanyi, J. Electrochem. Soc. **133**, 1607 (1986).
[45]A. L. Margaryan, V. M. Arutyunyan, and Zh. R. Panosyan, Uch. Zap. Erevan Gos. Univ. No. 2(159), 148 (1985).
[46]A. L. Margaryan, Zh. R. Panosyan, V. M. Arutyunyan, and V. A. Meliksetyan, Abstracts of Papers presented at Tenth All-Union Conf. on Physics of Semiconductors [in Russian], Vol. 3, Minsk, 1985, p. 91.
[47]A. R. Mailyan, Author's Abstract of Thesis for the Degree of Candidate of Physicomathematical Sciences [in Russian], Odessa, 1987.
[48]V. M. Arutyunyan, *Generation–Recombination Effects and Double Injection in Semiconductors* [in Russian], Izd. Akad. Nauk Arm. SSR, Erevan, 1977.
[49]G. P. Peka, *Physical Effects on the Surfaces of Semiconductors* [in Russian], Vishcha Shkola, Kiev, 1984.
[50]A. V. Sachenko and O. F. Snitko, *Photoelectric Effects in Surface Layers of Semiconductors* [in Russian], Naukova Dumka, Kiev, 1984.
[51]M. Cardona, *Optical Modulation Spectroscopy of Solids*, Suppl. 11 to Solid State Phys., Academic Press, N. Y., 1969.
[52]V. A. Tyagaĭ and O. V. Snitko, *Electroreflection of Light in Semiconductors* [in Russian], Naukova Dumka, Kiev, 1980.
[53]R. P. Silberstein, F. H. Pollak, J. K. Lyden, and M. Tomkiewicz, Phys. Rev. B **24**, 7397 (1981).
[54]R. P. Silberstein, J. K. Lyden, M. Tomkiewicz, and F. H. Pollak, J. Vac. Sci. Technol. **19**, 406 (1981).
[55]P. Lemasson, J. P. Dalbera, and J. Gautron, J. Appl. Phys. **52**, 6296 (1981).
[56]W. Siripala and M. Tomkiewicz, Phys. Rev. Lett. **50**, 443 (1983).
[57]M. Tomkiewicz and W. Siripala, J. Electrochem. Soc. **131**, 736 (1984).
[58]M. Tomkiewicz, J. Photochem. **29**, 165 (1985).
[59]V. M. Arutyunyan *et al.*, in *Physics and Technical Applications of II-VI Semiconductors* [in Russian], Vol. 1, Vilnius Technical College, 1983, p. 140.
[60]Zh. R. Panosyan, A. R. Mailyan, and A. O. Arakelyan, Fiz. Tverd. Tela (Leningrad) **27**, 1526 (1985) [Sov. Phys. Solid State **27**, 918 (1985)]; Zh. R. Panosyan, A. A. Pogosyan, and V. A. Meliksetyan, Fiz. Tverd. Tela (Leningrad) **27**, 1866 (1985) [Sov. Phys. Solid State **27**, 1120 (1985)]; Zh. R. Panosyan, Z. A. Kasamanyan, and A. R. Mailyan, Pis'ma Zh. Eksp. Teor. Fiz. **41**, 251 (1985) [JETP Lett. **28**, 857 (1986)].
[61]Zh. R. Panosyan, A. L. Margaryan, and V. M. Arutyunyan, Fiz. Tverd. Tela (Leningrad) **28**, 1518 (1986) [Sov. Phys. Solid State **28**, 857 (1986)].
[62]A. A. Pogosyan, V. M. Arutyunyan *et al.*, Fizika (Erevan) No. 8, 123 (1987).
[63]E. I. Rashba and M. D. Sturge (Eds.), *Excitons*, North-Holland, Amsterdam, 1982. [Russ. transl., Mir, M., 1985]
[64]D. Peramunage, W. Siripala, M. Tomkiewicz, and D. S. Ginley, Chem. Phys. Lett. **99**, 479 (1983).
[65]O. A. Aktsipetrov and E. D. Mishina, Dokl. Akad. Nauk SSSR **274**, 62 (1984) [Sov. Phys. Dokl. **29**, 37 (1984)]; O. A. Aktsipetrov, I. M. Baranova, and E. D. Mishina, Dokl. Akad. Nauk SSSR **296**, 1348 (1987) [Sov. Phys. Dokl. **32**, 839 (1987)].
[66]J. A. Turner, J. Manassen, and A. J. Nozik, Appl. Phys. Lett. **37**, 488 (1980).
[67]A. J. Nozik in *Photovoltaic and Photoelectrochemical Solar Energy Conversion* (Proc. NATO Advanced Study Institute, Gent, Belgium, 1980, ed. by F. Cardon, W. P. Gomes, and W. Dekayser), Plenum Press, N. Y., 1981, p. 263.
[68]J. A. Turner, J. Manassen, and A. J. Nozik, *Photoeffects at Semiconductor–Electrolyte Interfaces* (ed. by A. J. Nozik), American Chemical Society, Washington, 1981, p. 253 [ACS Symposium Series No. 146].
[69]A. J. Bard, F. A. Fan, A. B. Bocarsly *et al.*, J. Am. Chem. Soc. **102**, 3671 (1980).
[70]A. J. Nozik, D. S. Boudreaux, and R. R. Chance, in *Interfacial Photoprocesses: Energy Conversion and Synthesis* (ed. by M. S. Wrighton), American Chemical Society, Washington, 1980, p. 155 [Advances in Chemistry Series, No. 184].
[71]F. Williams and A. J. Nozik, Nature (Lonon) **271**, 137 (1978).
[72]D. S. Boudreaux, F. Williams, and A. J. Nozik, J. Appl. Phys. **51**, 2158 (1980).
[73]E. Buhks and F. Williams, in *Photoelectrochemistry: Fundamental Processes and Measurement Techniques* (ed. by W. L. Wallace, A. J. Nozik, S. K. Deb, and R. H. Wilson), Electrochemical Society, Penningon, N.J., 1981, p. 1.
[74]J. A. Turner and A. J. Nozik, Appl. Phys. Lett. **41**, 101 (1982).
[75]G. Cooper, J. A. Turner, B. A. Parkinson, and A. J. Nozik, J. Appl. Phys. **54**, 6463 (1983).
[76]R. T. Ross and A. J. Nozik, J. Appl. Phys. **53**, 3813 (1982).
[77]É. I. Rashba, Z. S. Gribnikov, and V. Ya. Kravchenko, Usp. Fiz. Nauk **119**, 3 (1976) [Sov. Phys. Usp. **19**, 361 (1976)].
[78]V. A. Volkov, V. A. Petrov, and V. B. Sandomirskiĭ, Usp. Fiz. Nauk **131**, 423 (1980) [Sov. Phys. Usp. **23**, 375 (1980)].
[79]T. Ando, A. W. Fowler, and F. Stern, Rev. Mod. Phys. **54**, 437 (1982).
[80]A. P. Silin, Usp. Fiz. Nauk **147**, 485 (1985) [Sov. Phys. Usp. **28**, 972 (1985)].
[81]A. J. Nozik, B. R. Thacker, and J. M. Olson, Nature (London) **316**, 51 (1985).
[82]A. J. Nozik, B. R. Thacker, J. A. Turner, and J. M. Olson, J. Am. Chem. Soc. **107**, 7805 (1985).
[83]A. J. Nozik, B. R. Thacker, J. A. Turner *et al.*, Appl. Phys. Lett. **50**, 34 (1987).

[84]R. Rossetti, J. L. Ellison, J. M. Gibson *et al.*, J. Chem. Phys. **80**, 4464 (1984).
[85]A. J. Nozik, F. Williams, M. T. Nedadović *et al.*, J. Phys. Chem. **89**, 397 (1985).
[86]J. M. Nedeljković, M. T. Nedanović, O. I. Mićić, and A. J. Nozik, J. Phys. Chem. **90**, 12 (1986).
[87]L. E. Brus, J. Chem. Phys. **80**, 4403 (1984).
[88]Al. L. Éfros and A. L. Éfros, Fiz. Tekh. Poluprovodn. **16**, 1209 (1982) [Sov. Phys. Semicond. **16**, 772 (1982)].
[89]A. I. Ekimov, A. A. Onushchenko, A. G. Plokhin *et al.*, Zh. Eksp. Teor. Fiz. **88**, 1490 (1985) [Sov. Phys. JETP **61**, 891 (1985)]; A. I. Ekimov, A. A. Onushchenko, M. E. Raĭkh *et al.*, Zh. Eksp. Teor. Fiz. **90**, 1795 (1986) [Sov. Phys. JETP **63**, 1054 (1986)].
[90]A. I. Ekimov and A. A. Onushchenko, Pis'ma Zh. Eksp. Teor. Fiz. **34**, 363 (1981) [JETP Lett. **34**, 345 (1981)].
[91]A. I. Ekimov and A. A. Onushchenko, Pis'ma Zh. Eksp. Teor. Fiz. **40**, 337 (1984) [JETP Lett. **40**, 1136 (1984)].
[92]A. Fujishima and K. Honda, Nature (London) **238**, 37 (1972).
[93]M. Tomkiewicz and H. Fay, Appl. Phys. **18**, 1 (1979).
[94]L. Peraldo Bicelli, Surf. Technol. **20**, 357 (1983).
[95]I. P. Lisovskiĭ and L. P. Terebezhnik, Optoelektron. Poluprovodn. Tekh. No. 9, 19 (1986).
[96]A. Heller, Science **223**, 1141 (1984).
[97]E. L. Johnson, Technical Digest of Intern. Electron Devices Meeting, Washington, DC, 1981, publ. by Institute of Electrical and Electronics Engineers, N. Y., 1981, p. 2; J. D. Luttmer and I. Trachtenberg, J. Electrochem. Soc. **132**, 1312 (1985).
[98]T. A. Vardapetyan, V. M. Arutyunyan *et al.*, Elektrotekh. Promst. Ser. Khim. Fiz. Istochn. Toka No. 3(96), 1 (1984).
[99]A. G. Sarkisyan, V. M. Arutyunyan, V. V. Melikyan, and É.V. Putnyn', Élektrokhimiya **22**, 511 (1986). [Sov. Electrochem. **22**, 475 (1986)].
[100]V. M. Arutyunyan *et al.*, Izv. Akad. Nauk Arm. SSR Fiz. **18**, 39 (1983).
[101]V. M. Arutyunyan, *et al.*, Uch. Zap. Erevan Gos. Univ. No. 1(153) 73 (1984).
[102]V. M. Arutyunyan, A. G. Sarkisyan, and G. E. Shakhnazaryan, Geliotekhnika No. 5, 3 (1985). [Appl. Sol. Energy (USSR) **21**, No. 5,1 (1985)]
[103]M. Matsumura, Y. Sakai, S. Sugahara *et al.*, Sol. Energy Mater. **13**, 57 (1986).
[104]C. D. Lokhande and S. H. Pawar, Mater. Chem. Phys. **11**, 201 (1984).
[105]S. Chandra and R. K. Pandey, Phys. Status Solidi A **72**, 415 (1982).
[106]T. A. Vardapetyan, L. A. Arutyunyan, and V. M. Arutyunyan, Geliotekhnika No. 1, 6 (1983). [Appl. Sol. Energy (USSR) **19**, No. 1, 4 (1983)].
[107]V. M. Autyunyan *et al.*, *Solar Photoelectric Energetics* [in Russian], Ylym, Ashkhbad (1983), p. 263.
[108]K. Honda, A. Fujishima, and T. Inoue, in Hydrogen Energy Progress (Proc. Third World Hydrogen Energy Conf., Tokyo, 1980, ed. by T. N. Veziroğlu, K. Fueki, and T. Ohta), Vol. 2, Pergamon Press, Oxford, 1981, p. 753.
[109]V. M. Arutyunyan and T. A. Vardapetyan, Geliotekhnika No. 2, 3 (1983). [Appl. Sol. Energy [USSR) **19**, No. 2, 1 (1983)]
[110]A. I. Kulak, *Electrochemistry of Semiconductor Heterostructures* [in Russian], Universitetskoe, Minsk, 1986.
[111]S. Wagner and J. L. Shay, Appl. Phys. Lett. **31**, 446 (1977); W. E. Pinson, Appl. Phys. Lett. **40**, 970 (1982).
[112]Research on Solar Energy Conversion by Means of Physical, Chemical and Biological Processes: Report, Part 2, Ministry of Education, Science, and Culture of Japan, Tokyo, 1983, p. 6.
[113]H. Ono, H. Morisaki, and K. Yazawa, Jpn. J. Appl. Phys. Part 1 **21**, 1075 (1982); H. Morisaki, H. Ono, H. Dohkoshi, and K. Yazawa, Jpn. J. Appl. Phys. Part 2 **19**, L148 (1980).
[114]R. C. Kainthla, B. Zelenay, and J. O'M. Bockris, J. Electrochem. Soc. **133**, 248 (1986).
[115]J. Gobrecht, R. Potter, R. Nottenburg, and S. Wagner, J. Electrochem. Soc. **130**, 2280 (1983).
[116]D. Belanger, J. P. Dodelet, and B. A. Lombos, J. Electrochem. Soc. **133**, 1113 (1986).
[117]J. A. Switzer, J. Electrochem. Soc. **133**, 722 (1986).
[118]O. M. R. Chyan, S. I. Ho, and K. Rajeshwar, J. Electrochem. Soc. **133**, 531 (1986).
[119]M. Noda, Int. J. Hydrogen Energy **7**, 311 (1982).
[120]W. Gissler, A. J. McEvoy, and M. Graetzel, J. Electrochem. Soc. **129**, 1733 (1982); W. Gissler and A. J. McEvoy, Sol. Energy Mater. **10**, 309 (1984); A. J. McEvoy and W. Gissler, J. Appl. Phys. **53**, 1251 (1982).
[121]Y. Nakato, Y. Iwakabe, M. Hiramoto, and H. Tsubomura, J. Electrochem. Soc. **133**, 900 (1986).
[122]A. T. Howe, R. T. Hawkins II, and T. H. Fleisch, J. Electrochem. Soc. **133**, 1369 (1986).
[123]M. Matsumura, H. Iwata, T. Inoue, and H. Tsubomura, Sol. Energy Mater. **14**, 475 (1986).
[124]L. P. Gor'kov, Usp. Fiz. Nauk **144**, 381 (1984) [Sov. Phys. Usp. **27**, 809 (1984)].
[125]G. A. Chamberlain, Sol. Cells **8**, 47 (1983).
[126]A. M. Hermann, Appl. Phys. Commun. **3**, 59 (1983).
[127]R. N. Noufi, Appl. Phys. Commun. **3**, 35 (1983).
[128]J. Simon, J. J. Andre, and A. Skoulious, Nouv. J. Chim. **10**(6), 295 (1986); J. Simon, F. Tournilhac, and J. J. Andre, Nouv. J. Chim. **11**(5), 383 (1987).
[129]T. Skotheim, L. G. Petersson, O. Inganas, and I. Lundström, J. Electrochem. Soc. **129**, 1737 (1982).
[130]T. Skotheim and I. Lundström, J. Electrochem. Soc. **129**, 894 (1982).
[131]R. Noufi, J. Electrochem. Soc. **130**, 2126 (1983).
[132]K. A. Daube, D. J. Harrison, T. E. Mallouk *et al.*, J. Photochem. **29**, 71 (1985).
[133]A. J. Frank and K. Honda, J. Photochem. **29**, 195 (1985).
[134]R. C. Hughes, D. S. Ginley, and A. K. Hays, Appl. Phys. Lett. **40**, 853 (1982).
[135]T. P. Henning and A. J. Bard, J. Electrochem. Soc. **130**, 613 (1983).
[136]S. K. Schmidt, R. L. Cook, and A. F. Sammels, J. Electrochem. Soc. **133**, 1617 (1986).
[137]O. Haas, N. Müller, and H. Gerischer, Electrochim. Acta **27**, 991 (1982).
[138]M. E. Langmuir, M. A. Parker, and R. D. Rauch, J. Electrochem. Soc. **129**, 1705 (1982).
[139]F. R. F. Fan, B. Reichman, and A. J. Bard, J. Am. Chem. Soc. **102**, 1488 (1980).
[140]C. R. Martin, I. Rubinstein, and A. J. Bard, J. Am. Chem. Soc. **104**, 4817 (1982).
[141]H. D. Abrunã and A. J. Bard, J. Am. Chem. Soc. **103**, 6898 (1981).
[142]A. I. Mazur and V.N. Grachev, *Electrochemical Tracers* [in Russian], Radio i Svyaz', M., 1985.
[143]O. Inganäs and I. Lundström, J. Electrochem. Soc. **131**, 1129 (1984).

Translated by A. Tybulewicz